JOURNAL OF GEOPHYSICAL RESEARCH: OCEANS, VOL. 118, 1–23, doi:10.1002/2013JC009164, 2013

Impact of sea-ice processes on the carbonate system and ocean acidification at the ice-water interface of the Amundsen Gulf, Arctic Ocean

Agneta Fransson,[1,2] Melissa Chierici,[3,4] Lisa A. Miller,[5] Gauthier Carnat,[6] Elizabeth Shadwick,[7,8] Helmuth Thomas,[7] Simon Pineault,[9] and Tim N. Papakyriakou[6]

Received 31 May 2013; revised 31 October 2013; accepted 26 November 2013.

[1] From sea-ice formation in November 2007 to onset of ice melt in May 2008, we studied the carbonate system in first-year Arctic sea ice, focusing on the impact of calcium-carbonate ($CaCO_3$) saturation states of aragonite (ΩAr) and calcite (ΩCa) at the ice-water interface (UIW). Based on total inorganic carbon (C_T) and total alkalinity (A_T), and derived pH, CO_2, carbonate ion ($[CO_3^{2-}]$) concentrations and Ω, we investigated the major drivers such as brine rejection, $CaCO_3$ precipitation, bacterial respiration, primary production and CO_2-gas flux in sea ice, brine, frost flowers and UIW. We estimated large variability in sea-ice C_T at the top, mid, and bottom ice. Changes due to $CaCO_3$ and CO_2-gas flux had large impact on C_T in the whole ice core from March to May, bacterial respiration was important at the bottom ice during all months, and primary production in May. It was evident that the sea-ice processes had large impact on UIW, resulting in a five times larger seasonal amplitude of the carbonate system, relative to the upper 20 m. During ice formation, $[CO_2]$ increased by 30 μmol kg^{-1}, $[CO_3^{2-}]$ decreased by 50 μmol kg^{-1}, and the ΩAr decreased by 0.8 in the UIW due to CO_2-enriched brine from solid $CaCO_3$. Conversely, during ice melt, $[CO_3^{2-}]$ increased by 90 μmol kg^{-1} in the UIW, and Ω increased by 1.4 between March and May, likely due to $CaCO_3$ dissolution and primary production. We estimated that increased ice melt would lead to enhanced oceanic uptake of inorganic carbon to the surface layer.

Citation: Fransson, A., M. Chierici, L. A. Miller, G. Carnat, E. Shadwick, H. Thomas, S. Pineault, and T. N. Papakyriakou (2013), Impact of sea-ice processes on the carbonate system and ocean acidification at the ice-water interface of the Amundsen Gulf, Arctic Ocean, *J. Geophys. Res. Oceans*, *118*, doi:10.1002/2013JC009164.

1. Introduction

[2] In the Arctic Ocean, polynyas and flaw leads in the sea ice continually form, not only as the result of sea-ice melt in the spring and summer, but throughout the year both around the continental margins and within the ocean interior [e.g., *Barber and Hanesiak*, 2004; *Barber et al*., 2010]. The Cape Bathurst Polynya, in Amundsen Gulf, south of Banks Island (Figure 1), is part of the circumpolar flaw-lead system that extends along the entire coastal Arctic Ocean [*Barber and Massom*, 2007] and is a site of sea-ice formation, associated brine rejection. The polynya generally freezes-up in October/November and reopens in June, exposing the surface water to the atmosphere and for CO_2 exchange, although it is not a very strong CO_2 sink [e.g., *Galley et al*., 2008; *Fransson et al*., 2009; *Shadwick et al*., 2011a; *Else et al*., 2011, 2012]. Nonetheless, the sea ice in Amundsen Gulf remains mobile throughout the winter, resulting in a continually changing ice cape consisting of a mixture of ice, open water, and newly forming ice [*Barber et al*., 2010], as well as air-sea CO_2 exchanges that can persist throughout the winter [*Else et al*., 2011, 2012].

[3] The various types of sea ice (i.e., very thin, rapidly freezing new ice; thicker first-year ice; and thick multiyear ice) may play different roles in the Arctic Ocean's response to climate change, not only through physical mechanisms [e.g., *Carmack et al*., 2006], but also through direct effects on CO_2 dynamics and vertical transport [e.g., *Rysgaard et al*., 2007; *Else et al*., 2011]. Sea-ice formation affects the water column by concentrating salt and other chemical substances in the water below the ice. During sea-ice formation, high-density brine is released into the underlying

[1]Norwegian Polar Institute, Fram Centre, Tromsø, Norway.
[2]Department of Earth Sciences, University of Gothenburg, Göteborg, Sweden.
[3]Institute of Marine Research, Tromsø, Norway.
[4]Department of Chemistry and Molecular Biology, Marine Chemistry, University of Gothenburg, Göteborg, Sweden.
[5]Institute of Ocean Sciences, Fisheries and Oceans Canada, Sidney, British Columbia, Canada.
[6]Center for Earth Observation Science, University of Manitoba, Winnipeg, Manitoba, Canada.
[7]Department of Oceanography, Dalhousie University, Halifax, Nova Scotia, Canada.
[8]Antarctic Climate and Ecosystems Cooperative Research Center, University of Tasmania, Hobart, TAS, Australia.
[9]Département de Biologie, Québec-Océan, Pavillon Vachon, Université Laval, Quebec, Canada.

Corresponding author: A. Fransson, Norwegian Polar Institute, Fram Centre, NO-9296 Tromsø, Norway. (agneta.fransson@npolar.no)

2169-9275/13/10.1002/2013JC009164

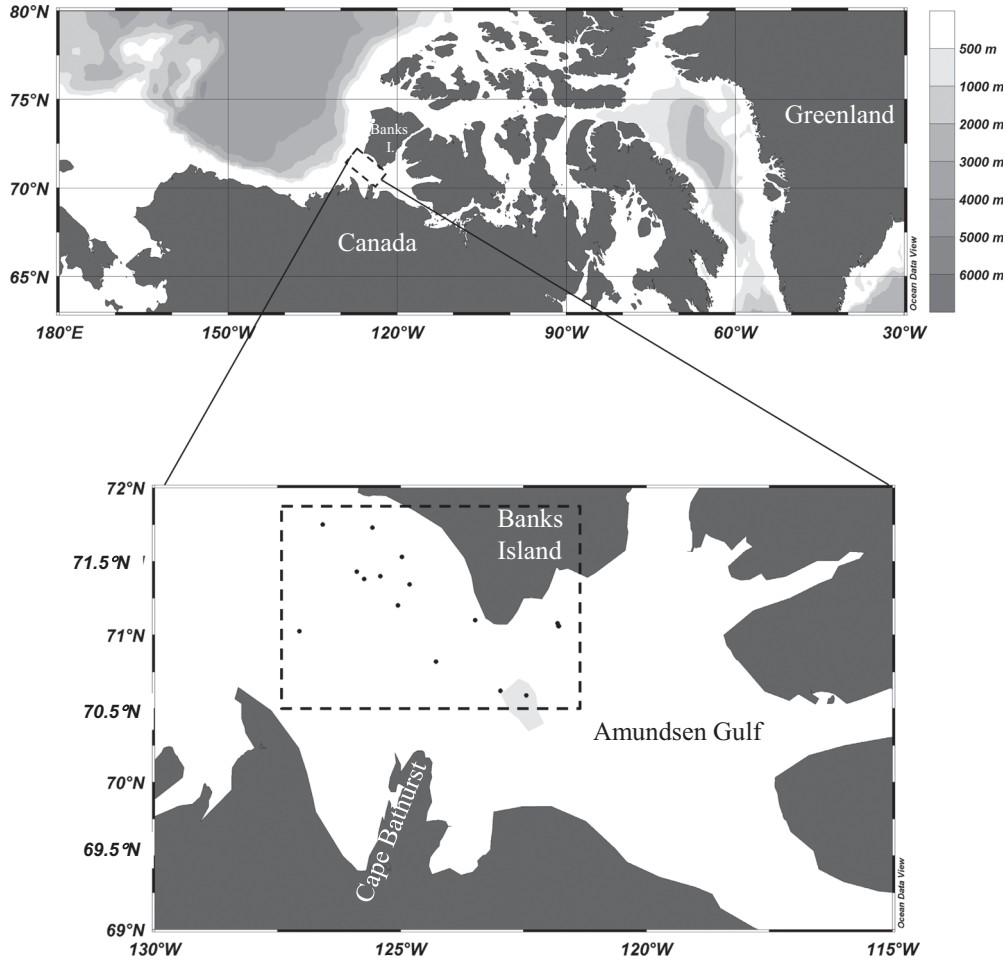

Figure 1. Map of the study area with all sea-ice sampling locations shown as black dots. The area within the dashed box is the region over which the seasonal variability analysis was applied (122°W–126°W, 70°N–71.5°N).

water at a rate dictated by sea-ice growth and phase relationships [e.g., *Cox and Weeks*, 1983]. In autumn and winter, the brine is enriched, with respect to the surface water, in chemical substances, including CO_2 and carbonate species, whereas in late spring and summer, the brine becomes diluted by melt water within the ice. Thus, an important aspect of cold-season brine rejection is the presence of relatively dense (saline) brine that appears underneath the ice. This dense water sinks in a process that provides a potential export pathway for carbon from the surface into deeper water layers [e.g., *Jones and Coot*, 1981; *Papadimitriou et al*., 2004; *Anderson et al*., 2004; *Rysgaard et al*., 2007].

[4] In addition to brine rejection, several processes in sea ice affect the content of total inorganic carbon, such as changes in salinity and temperature, primary production, bacterial respiration, gas exchange, and $CaCO_3$ precipitation and dissolution [e.g., *Fransson et al*., 2011]. The variability of carbon transport and the effect of biological processes in the sea ice are poorly understood but have a strong potential to affect the CO_2 transport and exchange with the surrounding environment. During primary production, CO_2 is assimilated, and during heterotrophic respiration, CO_2 is released. The temperature affects the CO_2 solubility, in that the solubility increases with decreasing temperature, and increased salinity (e.g., during ice-brine formation) decreases the solubility. Calcium carbonate ($CaCO_3$) precipitation during ice formation releases CO_2 to the aqueous phase:

$$Ca^{2+} + 2HCO_3^- \Longleftrightarrow CaCO_3(s) + H_2O + CO_2(aq) \qquad (1)$$

[5] The solid $CaCO_3$ may be left in the ice until the onset of melt, melting or when the ice becomes porous enough to release the $CaCO_3$ to the underlying water [e.g., *Lyakhin*, 1970]. Solid $CaCO_3$, in the form of ikaite (formula $CaCO_3 \cdot 6(H_2O)$, has been found in Arctic and Antarctic sea ice [e.g., *Dieckmann et al*., 2008, 2010; *Rysgaard et al*., 2012, 2013; *Nomura et al*., 2013; *Geilfus et al*., 2013], and several studies have found evidence of $CaCO_3$ precipitation in the sea ice [e.g., *Rysgaard et al*., 2007; *Fransson et al*., 2011; *Miller et al*., 2011b; *Geilfus et al*., 2012]. $CaCO_3$ in sea ice precipitates under the form of ikaite [e.g., *Dieckmann et al*., 2008]. Ikaite is formed in cold, saline waters where the formation of calcite is inhibited, and it decomposes into water and calcite above 4°C [*Assur*, 1958]. Above a given brine-volume threshold (above 5% for ideal, columnar ice) [*Golden et al*., 2007], chemical substances

dissolved in sea-ice brine are highly movable [*Cox and Weeks*, 1983; *Loose et al*., 2009, 2010]. Gas-bubble transport in brine channels is thought to be possible above a brine-volume threshold of approximately 7.5% [*Zhou et al*., 2013]. The trend in the ratio of total alkalinity (A_T) to total inorganic carbon (C_T) (A_T:C_T) in the water below the sea ice can be an useful indicator of calcium carbonate ($CaCO_3$) precipitation or dissolution [e.g., *Rysgaard et al*., 2007]. A decreasing A_T:C_T ratio in the UIW and brine reflects $CaCO_3$ precipitation in the sea ice during ice formation and CO_2 increases in the brine. Conversely, during ice melt, $CaCO_3$ dissolves as CO_2 is consumed.

[6] The impact of increasing CO_2 concentrations on the acidification state of the Arctic Ocean is currently a critical field of investigation [e.g., *Chierici and Fransson*, 2009; *Yamamoto-Kawai et al*., 2009; *Azetzu-Scott et al*., 2010; *Chierici et al*., 2011; *Shadwick et al*., 2011b]. Increased CO_2 in the ocean has led to decreases in carbonate-ion concentrations ($[CO_3^{2-}]$) and the calcium-carbonate saturation of aragonite (ΩAr) and calcite (ΩCa) as follows:

$$\Omega = \frac{[CO_3^{2-}]sw \times [Ca^{2+}]sw}{K_{sp}} \quad (2)$$

where the "sw" subscript denotes concentrations measured in seawater, K_{sp} is the condition equilibrium constant at a given salinity, temperature, and pressure. $[Ca^{2+}]$ is calcium-ion concentration, which is proportional to salinity in seawater, according to *Mucci* [1983]. When $\Omega < 1$, solid $CaCO_3$ is chemically unstable and prone to dissolution (i.e., the waters are undersaturated with respect to the $CaCO_3$ mineral), and when $\Omega > 1$, solid $CaCO_3$ is stable in the solid state and theoretically could even form abiotically (i.e., the solution is supersaturated). *Chierici et al*. [2011] and *Chierici and Fransson* [2009] found that in the Canadian Arctic Archipelago, the $CaCO_3$ saturation state of the surface water varied depending on location and season and was closely related to variations in biogeochemical processes. These studies also found aragonite-undersaturated surface waters on the freshwater-influenced shelves of the western Arctic Ocean in summer 2005, substantially sooner than predicted by recent dynamic models [*Orr et al*., 2005; *Steinacher et al*., 2009]. *Chierici et al*. [2011] found that the aragonite-saturation state in the polar mixed layer under the winter ice in Amundsen Gulf decreased, as a result of increased CO_2 due to mineralization of organic matter. However, they did not explicitly investigate the effect of sea-ice processes on the $CaCO_3$ saturation at the ice-water interface and in underlying water.

[7] There have been a few studies of the winter sea-ice carbonate system, and little is known about the seasonal evolution of inorganic-carbon dynamics in sea ice during sea-ice formation, from autumn to spring [*Miller et al*., 2011b]. Similarly, the effect of sea-ice processes on underlying water carbonate chemistry and the calcium-carbonate ($CaCO_3$) saturation state (Ω) of aragonite and calcite in the Arctic Ocean are not well known. To our knowledge, this is the only study in the Arctic Ocean focusing on the full carbonate system at the ice-water interface. In this study, we use unique winter and spring data from Arctic sea ice, under-ice water, brine, frost flowers, and snow to: (1) investigate the evolution of inorganic carbon and nutrients in sea ice and underlying water during sea-ice formation; (2) determine the role of sea-ice processes in inorganic carbon transport to the underlying water and the effect on the ocean acidification (i.e., $CaCO_3$ saturation state); (3) consider other processes affecting C_T and A_T in the sea ice, such as $CaCO_3$ precipitation/dissolution, biological production, air-ice-water CO_2 exchange; and (4) estimate the effect of ice melt on the summer carbonate system and air-sea CO_2 fluxes.

2. Study Area

[8] We performed this study using the ship CCGS Amundsen as scientific platform from 14 November 2007 to 6 May 2008 as part of the Circumpolar Flaw Lead System (CFL) study, an International Polar Year project in the Amundsen Gulf [*Barber et al*., 2010, Figure 1]. We used archived ice chart data from the Canadian Ice Services (CIS) and satellite images, derived from the Advanced Microwave Scanning Radiometer (AMSR-E) daily sea-ice charts downloaded from the University of Bremen [*Spreen et al*., 2008], to describe the ice conditions from November 2007 to May 2008, and to determine the seasonal evolution of overall sea-ice coverage in the study region. In 2007, sea ice had started to form southwest of Banks Island by October 1 and by mid-October, 40–60% of the area was ice-covered. Except for a patch of open water in central Amundsen Gulf, 90% of the area was ice-covered by the last week of October. Ice covered nearly the whole area 1 week later. In Amundsen Gulf, the ice remained mobile throughout the winter-spring with a lot of open water, allowing new, rapid ice formation to continue. At the end of April, the area was completely ice covered again (90–100%). These conditions prevailed until May, when the sea ice started to melt, and until break-up at the end of June. The coldest air temperatures of approximately −25°C occurred in March 2008 (Table 1).

3. Methods

3.1. Sample Collection

[9] We sampled bulk sea ice (hereafter referred to as sea ice), brine, frost flowers, and under-ice water (UIW; the ice-water interface mainly collected between 0.1 and 2 m below the ice for analyses of CO_2-system parameters). At a few occasions, we sampled also UIW to 5 m depth. The study was focused on two periods of sea-ice formation: from 14 November to 14 December; and from 17 March to 6 May (onset of melt). Positions, dates, and physical characteristics of the sea-ice stations are summarized in Table 1.

[10] Sea ice was collected of one or two ice cores at each site using an ice corer (Kovacs© Mark II barrel ice auger, diameter = 0.09 m). For the carbonate system, each core was sectioned with a stainless steel saw into 10–20 cm sections. The ice sections were immediately transferred to gas-tight bags (Tedlar©; polyvinyl fluoride; CO_2 permeability estimated to be 4.3 $cm^3 \cdot mm/m^2 \cdot day^1 \cdot atm^1$ at 25°C) [*Massey*, 2003], which were immediately sealed with a clamp. Before sealing the bottle, 250 µL saturated mercuric chloride solution was added to approximately 1000 mL melted sample (corresponded to each sea-ice section), to halt

Table 1. Sampling Dates and Locations of the First-Year Sea-Ice Cores, Including Ice Thickness, Snow Depth, Freeboard, and Air Temperature[a]

Date (dd/mm/yy)	Latitude (°N)	Longitude (°W)	Ice Thickness (cm)	Snow Depth (cm)	Freeboard (cm)	Air Temperature (°C)
14/11/07[b]	70.07	125.04	36*	n.d.	3	−11.2
19/11/07	70.62	122.97	46*	2	2	−15.2
22/11/07	71.75	126.58	56*	2	5	−14.2
28/11/07	70.82	126.38	52*	5	3	−16
02/12/07	71.73	125.57	33*	4	n.d.	−18.2
06/12/07	71.32	124.79	37*	n.d.	4	−22
12/12/07	71.38	125.74	57	n.d.	n.d.	−22
14/12/07	71.43	125.89	63	n.d.	n.d.	−17
17/03/08[b]	71.10	123.48	130	10	10	−25
22/03/08[b]	71.06	121.78	135	10	10	−25.5
24/03/08	71.08	121.81	43*	n.d.	n.d.	−20.7
25/03/08	71.06	121.79	145	10	10	−25
26/03/08	71.06	121.79	50*	n.d.	n.d.	−25
26/03/08	71.06	121.79	40	n.d.	n.d.	−25
28/03/08	71.06	121.79	55	2	5	−24.2
28/03/08	71.06	121.79	140	10.5	3	−24.2
31/03/08	71.06	121.79	145	3	14	−20.7
31/03/08	71.06	121.79	55*	2	5	−20.7
26/04/08[b]	70.59	122.44	132	n.d.	n.d.	−10
29/04/08[b]	70.59	122.44	160	n.d.	n.d.	−11
02/05/08	70.82	124.28	141*	n.d.	n.d.	−5
06/05/08	71.03	127.06	80	n.d.	n.d.	−5

[a]The asterisk (*) denotes replicate cores collected <5 m apart from each other, and n.d. denotes no data. Note that under-ice water (0–2 m) was collected at all stations.
[b]Not included in the process study.

biological activity. The head-space air was gently removed from the small spigot on the bag, using a small hand pump (e.g., a Nalgene 6132 Repairable Hand Operated Vacuum pump). In November and December, the cores were cut into 5 cm sections for the top 15 and bottom 5 cm, with 10 cm sections in the interior of the ice [*Miller et al*., 2011a]. To get enough sample volume, two cores were taken at each site in order to combine two 5 cm sections in one bag. The 10 cm sections were individually bagged to provide sets of duplicates. In May, the ice cores were usually cut into three 30 cm sections. Replicate cores were sampled at several occasions which are denoted in Table 1. Occasionally, the cold and harsh weather conditions in March and April did not allow us to handle the bags in the field, and we were forced to bag the samples onboard the ship immediately after ice-core extraction. The sea-ice samples were slowly melted in darkness, reaching a temperature of approximately 4°C before careful transfer to borosilicate glass bottles using a silicon tube as to avoid contact with surrounding air. Glass bottles were sealed with glass stoppers or air-tight screw caps. The melted ice samples were stored in the dark, at 4°C, until analysis. At temperatures above 4°C, solid calcium carbonate dissolves. At analysis or transfer to bottles, the temperature was above 4°C and $CaCO_3$ was probably dissolved and hence we did not observe any solid $CaCO_3$ in our samples. However, we used fractionations (A_T:S and A_T:C_T) and changes in A_T to trace solid $CaCO_3$, already dissolved in the melted sample [*Rysgaard et al*., 2007; *Fransson et al*., 2011].

[11] In March and April, in parallel to the cores for carbonate system and salinity samples, we collected ice cores for nutrient analyses from the bottom parts (0–3, 3–7, and 0–10 cm) of cores and placed the cut sections in dark, isothermal containers for transportation back to the ship. Prefiltered surface seawater (FSW) (100 mL for every centimeter of ice core) was added to the nutrient sub-cores to minimize osmotic stress during melting [*Garrison and Buck*, 1986]. Melted sea-ice samples were collected in acid-washed 15 mL tubes. Large particles were removed by filtration through a 0.7 μm GF/F glass fiber filter mounted on a filter holder attached to a syringe. Samples were stored in the dark at 4°C and analyzed within 24 h.

[12] Sea-ice temperature was measured on site, immediately after the ice core was recovered, at 5 cm intervals using a handheld digital thermistor (Testo 720) with the precision of ±0.1°C and accuracy of ±0.2°C. The holes for the temperature measurement were carefully drilled along the core length, to avoid additional heating from the drill.

[13] For brine samples, holes were partially drilled to different depths (between 20 and 50 cm) in the sea ice (i.e., sackholes), using the ice corer (Kovacs© Mark II barrel ice auger, diameter = 0.09 m), and left to accumulate brine from the surrounding ice. The volume of brines collected varied between 30 mL (in March) and 300 mL (in May), depending mainly on ice temperature. The sackholes were covered with insulating lids of 2.5 cm thick rigid polystyrene foam (wrapped in polyethylene plastic sheeting), which were sealed with snow packed around the edges, to limit gas exchange with the atmosphere. We generally limited the brine-collection period to <30 min, although longer periods were sometimes required to accumulate sufficient brine during the coldest period in March and April, and hence those samples were particularly

susceptible to gas exchange. We used a syringe and surgical tubing to collect the brines from the sackholes and immediately transferred the brine samples to gas-tight borosilicate glass bottles. The temperature of brine was measured in the sackhole before the transfer to sample bottles, which were stored in an insulated container at 4°C to prevent freezing.

[14] Frost flowers were sampled approximately 500 m from the ship, between 2 and 20 m from the ice-core site using a Teflon ladle from a surface area of 1–2 m^2 for each sample. The samples were packed in Tedlar© bags and preserved by adding 120 μL saturated mercuric chloride ($HgCl_2$) solution to approximately 500 mL melted sample. After emptying the bags of surrounding air, the frost-flower samples were slowly thawed in darkness at a temperature of approximately 4°C, subsequently transferred to borosilicate glass bottles with glass stoppers, and stored cool and dark until analysis. Snow samples were sampled between 2 and 10 m from core-sampling site and were treated in the same way as the frost flowers.

[15] For UIW sampling at depths of 0.1–2 m below the ice-water interface, we used an electric submersible pond pump (e.g., Pondmaster, Supreme MD2, maximum flow of 12 L/min) and polyvinylchloride tubing (inner diameter 12.5 mm) within the core hole, at approximately the bottom of the ice. On a few occasions, samples were also collected from 5 m below the ice. The UIW samples were collected in 250 mL glass bottles with overflow to rinse (one full volume), sealed temporarily in the field using greased ground glass stoppers, and stored in an insulated container at 4°C to prevent freezing. The UIW temperature was measured in the sample bottle immediately after sampling on site using a handheld probe (Testo 720). The UIW samples were reopened and preserved with 60 μL of a saturated $HgCl_2$ solution added to 250 mL sample to halt biological activity. The bottled samples were stored in the dark at 4°C until analysis. UIW was always collected in parallel to the ice-core sampling site, maximum 10 m away.

[16] Subsurface samples (greater than 10 m) were collected through the ship CCGS Amundsen's moonpool. The moonpool was an opening in the ship's hull where instruments were deployed and seawater samples collected to prevent samples and equipment from freezing. For seawater sampling, we used a General Oceanics 24-bottle rosette of 12 L Niskin bottles equipped with a conductivity-temperature-depth sensor (CTD, Seabird SBE-911 plus), using standard protocols [*Dickson et al*., 2007]. Sites for sea ice, brine, UIW, and frost-flower sampling were between 100 m and 1 km apart from the water sampling onboard the ship to avoid disturbance.

3.2. Sample Analyses

[17] Following water collection and ice melt, the salinity of all the samples was measured using a conductivity meter (WP-84TPS meter), with a precision and accuracy of ±0.1 %. The total inorganic carbon (C_T) and total alkalinity (A_T) samples were generally analyzed within 12 h after thawing was completed. Analytical methods for C_T and A_T determination have been fully described in *Dickson et al*. [2007]. Briefly, all C_T and A_T samples were analyzed onboard the ship by coulometric and potentiometric titration, respectively. All C_T and some A_T analyses used a Versatile Instrument for the Determination of Titration Alkalinity (VINDTA 3C, Marianda), and some A_T was also measured using an automated Radiometer® potentiometric titrator [*Mucci et al*., 2010]. The average standard deviation for A_T, determined from replicate sample analyses from one sample bottle, and replicate cores when available (see Table 1 for replicate cores), was within ±1 μmol kg^{-1} for UIW and seawater samples. For sea-ice melt water, melted frost flowers and brine samples, the replicate samples were within ±3 μmol kg^{-1}. The average standard deviation for C_T, determined from replicate sample analyses from one sample bottle, was within ±1 μmol kg^{-1} for all sample varieties. Routine analyses of certified reference materials (CRM, provided by A. G. Dickson, Scripps Institution of Oceanography) ensured the accuracy of the measurements, which was better than ±1 μmol kg^{-1} and ±2 μmol kg^{-1} for C_T and A_T, respectively.

[18] The nutrient concentrations of nitrite ($[NO_2^-]$), nitrate ($[NO_3^-]$), phosphate ($[PO_4^{2-}]$), and silicate ($[SiO_2]$) were analyzed in liquid phase. Colorimetric determinations of nitrate + nitrite, nitrite and of soluble reactive phosphorus and orthosilicic acid (hereafter abbreviated as phosphate and silicic acid) were performed on an Autoanalyzer 3 (Bran & Luebbe) with routine methods adapted from *Grasshoff et al*. [2009]. Analytical detection limits were 0.05 μmol L^{-1} for nitrate + nitrite, 0.02 μmol L^{-1} for nitrite, and 0.05 and 0.1 μmol L^{-1} for phosphate and silicic acid, respectively. The concentrations of nutrients in melted ice cores were postcorrected for dilution by the added FSW.

[19] We used C_T, A_T, salinity, temperature, and depth for each sample as input parameters in a CO_2-chemical speciation model (CO2SYS program) [*Pierrot et al*., 2006] to calculate the calcium-carbonate saturation states (Ω) for aragonite (ΩAr) and calcite (ΩCa), carbon dioxide concentration ($[CO_2]$), CO_2 fugacity and partial pressure (fCO_2, pCO_2), and carbonate-ion concentration ($[CO_3^{2-}]$). We used the total hydrogen-ion scale (pH_T), the HSO_4^- dissociation constant of *Dickson* [1990], *Mucci* [1983] for the solubility products of aragonite and calcite, and the CO_2-system dissociation constants (K^*_1 and K^*_2) estimated by *Roy et al*. [1993, 1994]. We estimated the difference in calculated $[CO_3^{2-}]$ and $[CO_2]$ for low-salinity water samples (i.e., melted sea-ice samples) using the different constants of *Roy et al*. [1993, 1994] and *Merhbach et al*. [1973], refit by *Dickson and Millero* [1987], which resulted in −0.5 μmol kg^{-1} difference in melted sea ice (i.e., bulk), which is insignificant in relation to our analytical precision and the variability in the natural sea-ice system. For high-salinity samples such as brine and melted frost flowers, the same comparison resulted in a difference of −0.2 μmol kg^{-1} for $[CO_2]$ and −0.6 μmol kg^{-1} for $[CO_3^{2-}]$, which is also insignificant. However, despite the agreement between these sets of constants, none of them are actually appropriate at the low temperatures in ice or the high salinities of ice brines and all of them could induce errors.

[20] The carbonate system in low-salinity samples, such as sea ice, will change due to addition of mercuric chloride with the pH of 3.5. Adding 120 μL mercuric chloride to 500 mL melted sea ice (salinity of 5), the sample pH changed by 0.01 pH units, corresponding to changes in C_T of between 2 and 4 μmol kg^{-1} depending on A_T

(A. Fransson and M. Chierici, unpublished data, 2013). This C_T change is insignificant in comparison to the accuracy of the analytical methods and the natural variability of the concentrations within the sea ice.

4. Results and Discussion

4.1. Evolution of Sea-Ice Properties During Ice Formation

4.1.1. Physical Properties in Sea Ice

[21] Ice thickness, snow depth, and freeboard for all ice sampling locations are presented in Table 1. Ice thickness varied throughout the study, ranging between 33 cm in November/December 2007 and 160 cm in April 2008. Freeboard varied between 3 and 5 cm, and no slushy layer was observed throughout the study, indicating that the ice was dry and not flooded by seawater. The snow depth was at a maximum of 8 cm in May, consistently lower during the other study months. Since the study covered mostly the ice-forming season, before melting took place, we assumed that no superimposed ice formed at the time of sampling.

[22] Figures 2(a)–2(f) show depth profiles of the physical characteristics of the sea ice ((a, b) ice salinity, (c, d) temperature, and (e, f) brine volume) for two periods from November to December 2007 and from March to May 2008. The salinity varied for individual ice cores throughout the study (Figures 2a and 2b). However, most ice cores displayed a typical C-shape pattern, typical of first-year ice [e.g., *Malmgren*, 1927; *Thomas and Dieckmann*, 2010] with higher salinities at the ice-air/snow (top ice) interface and at the ice-water interface (bottom ice) than in the ice interior. This was also observed by *Geilfus et al*. [2012] in another study. The mean sea-ice salinity between November and December was 8.2 ± 2.1, and between March and May 6.9 ± 2.9.

[23] Ice temperatures were lowest at the ice-air interface, reflecting the influence of air temperature (Figures 2c and 2d). The temperature increased almost linearly toward the ice-water interface, where temperatures were close to the seawater freezing point (-2°C). Although the ice temperatures began to rise in March, the ice column was not yet isothermal by the time we stopped our sampling in May.

[24] We calculated brine-volume fraction (BV; Figures 2e and 2f) from bulk-ice salinity (S) and ice temperature (T, °C), according to *Frankenstein and Garner* [1967] derived from *Assur* [1958], according to

$$\mathrm{BV} = \frac{S}{1000}\left(\frac{49.185}{ABS(T)} + 0.532\right) \tag{3}$$

[25] As BV decreases, the ice becomes less permeable [e.g., *Golden et al*., 2007; *Loose et al*., 2009, 2010], and both gas and liquid transport decreases. Ice temperature fundamentally controls the ice porosity [*Petrich and Eicken*, 2010]. Brines and inorganic carbon were probably more mobile in the ice in November and December, when the ice was warmer and the BV was higher (Figure 2e) than during the coldest period of March and April, when BV was lower (Figure 2f). In the warmer ice in the bottom parts of the ice cores the porosity was high throughout our study. In a few newly formed ice cores (thickness <70 cm) in March and May, the measured ice temperatures were higher, implying high BV values throughout the ice (Figure 2f). This indicates that gas and brine could have been mobile within the ice. Brine can move vertically both downward and upward, and consequently inorganic carbon and salts can be transported in both directions. The downward transport of brine is caused by gravity and the upward transport by ice formation near base of ice layer, reducing the permeable channels, and hence squeezes brines upward by hydrostatic pressure. The downward-transported brine would finally end up in the underlying water and the upward-transported brine would end up at the ice surface, in some cases allowing the formation of frost flowers [*Perovich and Richter-Menge*, 1994; *Alvarez-Aviles et al*., 2008] and/or outgassing. The brine concentrations are integrated values and could give approximate estimates on changes over time in salinity and chemical substances extracted from the bulk ice to the brine channels.

4.1.2. Chemical Properties in Sea Ice

[26] Depth profiles of ice C_T and A_T (Figures 3a–3d) largely followed salinity (Figures 2a and 2b) with higher values at the ice-snow interface and at the ice-water interface, with lower values in the midparts. The carbonate-ion concentration ($[CO_3^{2-}]$) profiles were C-shaped in November and December (Figure 3e) with the highest values at the ice-snow interface. Concentrations became much more variable and lower from March to May (Figure 3f). From November to December, the CO_2 concentrations were relatively low (Figure 3g), possibly due to loss from the relatively warm ice to the air and underlying water. By March and May, the CO_2 concentrations and variability had increased, reaching maximum CO_2 values up to 20 μmol kg^{-1} (Figure 3h).

[27] At a few ice stations in March and April, sea-ice nutrient concentrations ($[NO_2^-]$, $[NO_3^-]$, $[PO_4^{2-}]$, and $[SiO_2]$) were measured in the bottom parts (0–3, 3–7, and 0–10 cm) of a couple of ice cores (Table 2). Over the month between 26 March and 26 April, nutrients increased in the bottom 3 cm of the ice (Table 2): $[NO_3^-]$ by 1.9 μmol L^{-1}, $[PO_4^{2-}]$ by 1.7 μmol L^{-1}, and $[SiO_2]$ by 12.9 μmol L^{-1}. According to project collaborators [*Nguyen and Maranger*, 2011], the nutrient increase was likely due to the release of nutrients by bacterial respiration in the bottom ice. Such increase showed bacterial respiration could also have been a significant CO_2 source, not only at the bottom of the ice but throughout the ice column [*Deming*, 2010]. Primary production was negligible between November and March due to limited light conditions and the concurrent absence of chlorophyll *a* in bottom ice [e.g., *Forest et al*., 2011; *Niemi et al*., 2011]. However, the primary production increased significantly toward mid-April and May [e.g., *Song et al*., 2011; *Pineault et al*., 2013]. In our study, the $[NO_3^-]$, $[PO_4^{2-}]$, and $[SiO_2]$ measured in the bottom ice section increased between the end of March and mid-April (Table 2), corresponding to C_T increases. *Ngyuen and Maranger* [2011] found that bacterial respiration outstripped primary production in February and March. As spring advanced, higher net primary production than bacterial respiration rate was measured in April and May. By mid-April and late April, primary production was significant according to *Ngyuen and Maranger* [2011], suggesting concomitant bacterial activity. Bacterial respiration was generally higher (more than three times) in the sea ice than at the ice-water interface (i.e., the UIW). The rate in the UIW increased toward the end of spring [*Nguyen and*

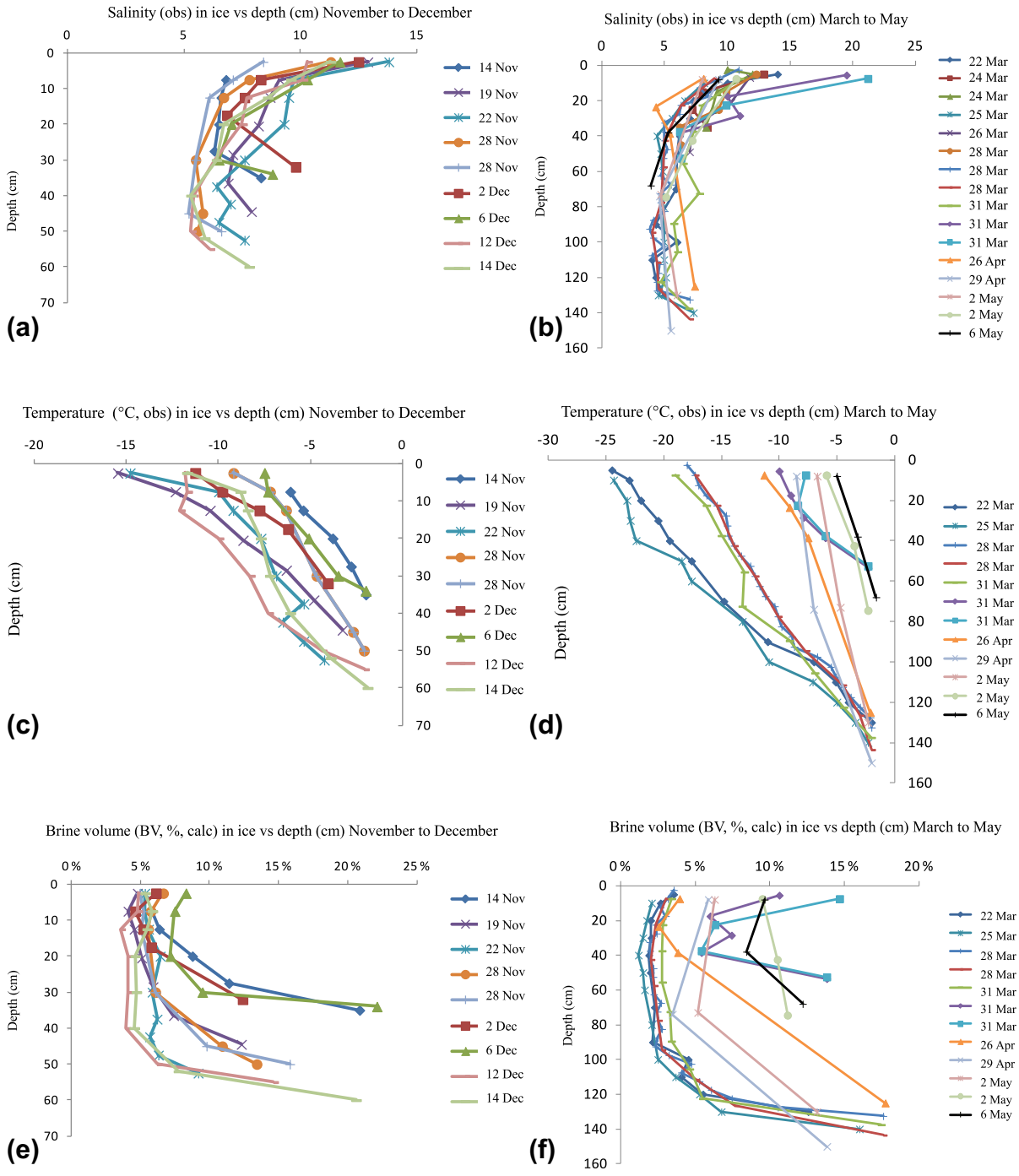

Figure 2. Vertical distribution of sea-ice physical properties: (a, b) bulk sea-ice salinity, (c, d, T °C) temperature, (e, f, BV, %) brine volume for two periods of ice formation; November–December 2007 and March to the beginning of May 2008. Ice cores collected at the same dates may be collected at different sites, reflected by differences in ice thickness and other properties between the two cores. "Obs" denotes that the values are measured and "calc" denotes that the values are calculated.

Maranger, 2011], which is consistent with our nutrient measurements (Table 2).

4.1.3. Properties in Brine, Under-Ice Water and Melted Frost Flowers

[28] Brine drained from the ice was enriched in salts, A_T, and C_T compared to the values in seawater (Table 3). The calculated pCO_2 was elevated between March and April. This would have facilitated release to the atmosphere or enhanced CO_2 gas exchange, if the brine volume and porosity were high enough. In general, brine volume was <5% for thick ice and >5% for thin ice. The average A_T:C_T ratio in brine was 1.08 for March to May, which does not clearly reflect the effect of $CaCO_3$ precipitation in the ice. However, the A_T:C_T ratio was extremely variable,

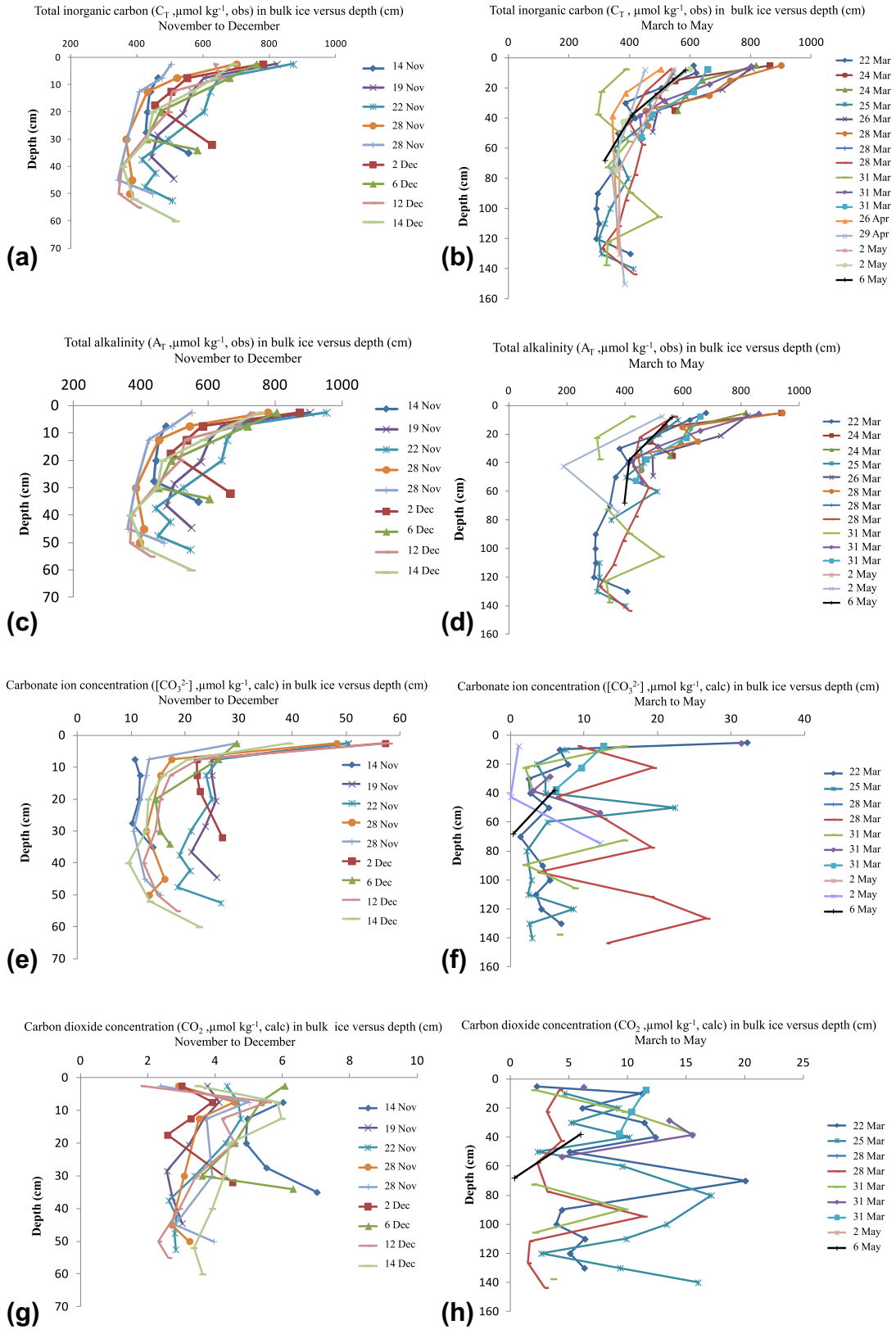

Figure 3. Vertical distribution of bulk sea-ice chemical properties: (a and b) total inorganic carbon (C_T, µmol kg^{-1}); (c and d) total alkalinity (A_T, µmol kg^{-1}); (e and f) carbonate ion concentration ([CO_3^{2-}], µmol kg^{-1}); and (g and h) carbon dioxide concentration (CO_2 µmol kg^{-1}), from November to December and March to May, respectively. Ice cores collected at the same dates may be collected at different sites, reflected by differences in ice thickness and other properties between the two cores. "Obs" denotes that the values are measured and "calc" denotes that the values are calculated.

Table 2. Concentrations of Nitrite ($[NO_2^-]$), Nitrate ($[NO_3^-]$), Phosphate ($[PO_4^{2-}]$), and Silicate ($[SiO_2]$) in Sea Ice and Under-Ice Water (UIW; 0–2 m), Stations, Sampling Date[a]

Sample	Date (dd/mm/yyyy)	Sample ID	$[NO_2^-]$ (μmol L^{-1})	$[NO_3^-]$ (μmol L^{-1})	$[SiO_2]$ (μmol L^{-1})	$[PO_4^{2-}]$ (μmol L^{-1})
Sea ice	18/03/2008	M3	n.d.	n.d.	n.d.	n.d.
Sea ice	23/03/2008	M3	0.03	1.29	2.11	0.24
Sea ice	26/03/2008	M3	0.05	1.76	2.78	0.40
Sea ice	26/04/2008	M3	0.08	3.68	15.7	2.12
Sea ice	18/03/2008	M7	n.d.	n.d.	n.d.	n.d.
Sea ice	23/03/2008	M7	<0.01	0.91	0.98	0.08
Sea ice	26/03/2008	M7	0.00	0.52	0.56	0.05
Sea ice	26/04/2008	M7	0.04	0.11	0.87	0.17
Sea ice	18/03/2008	M10	n.d.	n.d.	n.d.	n.d.
Sea ice	23/03/2008	M10	<0.01	0.99	1.22	0.11
Sea ice	26/03/2008	M10	0.01	0.83	1.13	0.14
Sea ice	26/04/2008	M10	0.05	1.20	5.42	0.77
UIW	17/03/2008	2 m	0.11	4.70	10.2	1.14
UIW	22/03/2008	2 m	0.16	4.28	8.58	1.02
UIW	25/03/2008	0 m	0.15	4.18	8.32	1.01
UIW	26/04/2008	0 m	0.07	2.92	8.90	n.d.

[a]M3 means bottom 3 cm (0–3 cm) of the ice core, M7 means 3–7 cm, and M10 means bottom 10 cm (0–10 cm), and n.d. denotes no data.

ranging between values of 2.7 in a sample collected in March and 1.2 in a sample from May, which could be the result of $CaCO_3$ precipitation. The calculated pH of in situ brine was relatively close to or higher than the values in seawater. The CO_2 gas concentrations ($[CO_2]$) in brine were up to six times higher than in UIW. In the brine, the aragonite saturation (ΩAr) increased drastically from low values of 0.2 in March to a supersaturation of 2.5 in May (Table 3). In the UIW, ΩAr was relatively constant, with an average value of 1.4.

[29] Frost flowers are formed on top of newly formed sea ice, by the freezing of upward-transported brine, creating a brine skim [e.g., *Perovich and Richter-Menge*, 1994]. New frost flowers are rich in chemical substances and bacteria [*Deming*, 2010; *Douglas et al*., 2012; *Granfors et al*., 2013]. In this study, measurements of A_T and C_T showed that $[CO_3^{2-}]$ was higher in melted frost-flower samples than in the ice brines or underlying water (Table 3). Coincidently, $[CO_2]$ was completely depleted in the frost-flower solutions, and pH corrected to in situ pH temperatures was relatively high, ranging between 9 and 11 (Table 3). The ΩAr in the frost flowers was largely supersaturated compared to that of surface water during the same period. The mean A_T:C_T ratio in the frost-flower melts varied between 1.6 and 2.2, which was higher than in the brine and the UIW (Table 3). The A_T values were enhanced relative to salinity (S), with A_T:S (87–97) larger than in brine (61–65) and UIW (70–71), suggesting solid $CaCO_3$ in the frost flowers.

4.2. Evolution of the Carbonate System and $CaCO_3$ Saturation in the Under-Ice Water

[30] Figure 4 shows the changes in the carbonate system of the UIW in the upper 2 m of the water column during two periods from November to December and from March to May (i.e., melt onset). In the UIW, brine rejection was the most significant sea-ice process explaining the changes of the carbonate system, as confirmed by the high salinities (Figure 4a), densities (not shown) and carbonate-system parameter concentrations in the top 2 m under the ice in March and April. This was also observed in the upper 60 m of the water column (polar mixed layer) during the CFL study [*Shadwick et al*., 2011a; *Chierici et al*., 2011]. Salinity increased by approximately 1.5 units in the UIW between the onset of ice formation (November/December) and before ice melt at beginning of May (Figure 4a). Increased concentrations was also observed in A_T and C_T, which increased by approximately 125 μmol kg^{-1} (Figures 4b and 4c). These increases in C_T and A_T were accompanied by rearrangement of the carbonate-system speciation so that the bicarbonate-ion concentration ($[HCO_3^-]$) increased by 125 μmol kg^{-1} (Figure 4d), $[CO_2]$ increased by 30 μmol kg^{-1} (Figure 4e) and carbonate-ion concentration ($[CO_3^{2-}]$) decreased by 50 μmol kg^{-1} (Figure 4f). Further, in situ pH decreased by 0.4 (Figure 4g), and pH^{25} at 25°C (temperature effect removed) decreased by 0.35 (Figure 4h) from November to April. In parallel with the $[CO_3^{2-}]$, the A_T:C_T ratio decreased in the UIW between November and April (Figure 4i) possibly due to the release of alkalinity-depleted brines from cold ice in which $CaCO_3$ had precipitated. During this process, the released CO_2 is dissolved and is more easily transported with the brine from the sea-ice drainage network to the UIW than the solid $CaCO_3$ [*Rysgaard et al*., 2013].

[31] The A_T:C_T ratio and pH values (both *in situ* and at 25°C) then increased to values above those in autumn as ice melt proceeded in May (Figure 4i) likely due to the combined effects of ice-melt water addition which contains excess A_T (and enhanced $[CO_3^{2-}]$; Figure 4f), loss of excess CO_2 from cold brine rejection (Figure 4e and Table 3), and primary production. The decrease in $[NO_3^-]$ at the ice-water interface, between the end of March and the end of April (Table 2), implies primary production and a corresponding biological carbon uptake. The early onset of carbon drawdown by primary production in mid-April was also confirmed by *Shadwick et al*. [2011a] and *Pineault et al*. [2013] using different approaches. During the onset of ice melt in May, $[CO_3^{2-}]$ was the only parameter that showed a net increase (Figure 4f), while A_T remained as high as during the onset of ice formation in November/

Table 3. Monthly Average Values and the Range Given as Minimum and Maximum Values Below Average Values (Min, Max) of Salinity, Temperature, and Carbonate-System Parameters in Melted Frost Flowers (FF; Brine Skim), Brine and Under-Ice Water (UIW)[a]

Month	Type	Salinity (min, max)	T in Situ (°C) (min, max)	A_T (μmol/kg) (min, max)	C_T (μmol/kg) (min, max)	pH in situ (min, max)	pCO_2 (μatm) (min, max)	HCO_3^- (μmol/kg) (min, max)	$[CO_3^{2-}]$ (μmol/kg) (min, max)	$[CO_2]$ (μmol/kg) (min, max)	ΩCa (min, max)	ΩAr (min, max)	A_T:C_T	A_T:S	N
Nov	FF	61	−15.6	5941	2677	10.7	2	505	2171	0.3	38	21	2.2	97	13
		(33.7, 76)	(−17, −14)	(2785, 9331)	(1688, 3664)	(9.5, 12)	(0, 7)	(13, 1081)	(777, 3651)	(0, 0.8)	(14, 65)	(8, 37)			
Dec	FF	44	−17	2331	1533	9.4	8	1059	473	1	11	7	1.6	53	2
		(22.5, 50)	(−19, −14)	(1597, 2785)	(1046, 1878)	(9.3, 9.7)	(3, 12)	(765, 1353)	(364, 787)	(0.4–1.6)	(9, 20)	(6, 12)			
March	FF	48	−23	4183	2503	9.5	7	1633	869	1	20	13	1.7	87	4
		(42, 54)	(−24, −21)	(3367, 5475)	(2188, 2905)	(9.5, 9.65)	(4, 9)	(1359, 1973)	(828, 930)	(0.8, 1.6)	(19, 21)	(12, 13)			
March	Brine	134	−8.1	9442	6854	9.4	1226	5493	1295	67	2	0.5	1.4	70	6
		(96, 169)	(−11, −6)	(6865, 13,673)	(4376, 8858)	(8.1, 12.1)	(0, 2469)	(283, 7651)	(204, 4093)	(0, 139)	(1, 4)	(0.1, 0.9)			
April	Brine	107	−6.2	6589	6495	8.1	3488	6164	149	182	1.0	0.3	1.0	62	13
		(70, 136)	(−9, −4)	(4857, 8191)	(4522, 8254)	(8.1, 8.9)	(548, 3519)	(4220, 7503)	(217, 737)	(27, 172)	(0.7, 4.5)	(0.1, 2.3)			
May	Brine	67	−2.7	4346	3994	8.2	648	3703	255	37	4.4	2.5	1.1	65	29
		(34, 73)	(−3.6, 0.5)	(2330, 4880)	(2229, 4670)	(7.97, 8.5)	(195, 1355)	(2116, 4409)	(85, 470)	(11, 74)	(2.1, 7.9)	(1.3, 4.6)			
Nov	UIW	30.1	−1.7	2131	2016	8.13	282	1907	89	20	2.2	1.35	1.06	71	9
		(30, 30.4)	(−1.8,−1.6)	(2120, 2154)	(2006, 2037)	(8.12, 8.15)	(275, 290)	(1898, 1924)	(86, 92)	(19, 20)	(2.1, 2.3)	(1.3, 1.4)			
Dec	UIW	30.4	−1.7	2155	2041	8.02	293	1932	88	20	2.1	1.3	1.06	71	27
		(30, 30.7)	(−2, −1.5)	(2126, 2178)	(2028, 2064)	(8.07, 8.14)	(277, 337)	(1904, 1959)	(79, 91)	(19, 23)	(1.9, 2.3)	(1.2, 1.4)			
March/ April	UIW	31.6	−1.8	2205	2130	7.95	484	2032	67	33	1.6	1.0	1.04	70	15
		(30.6, 32.4)	(−1.9, −1.8)	(2108, 2285)	(2079, 2178)	(7.74, 8.10)	(320, 736)	(1994, 2076)	(38, 90)	(22, 51)	(0.9, 2.2)	(0.6, 1.4)			
May	UIW	31.4	−1.1	2246	2105	8.16	281	1981	106	19	2.6	1.6	1.07	71	13
		(30.7, 32.1)	(−1.9, −0.6)	(2203, 2287)	(2028, 2149)	(8.09, 8.28)	(204, 332)	(1883, 2030)	(90, 131)	(13, 22)	(2.2, 3.2)	(1.4, 2.0)			

[a]Frost flowers also include frost-flowered snow introducing large variability.

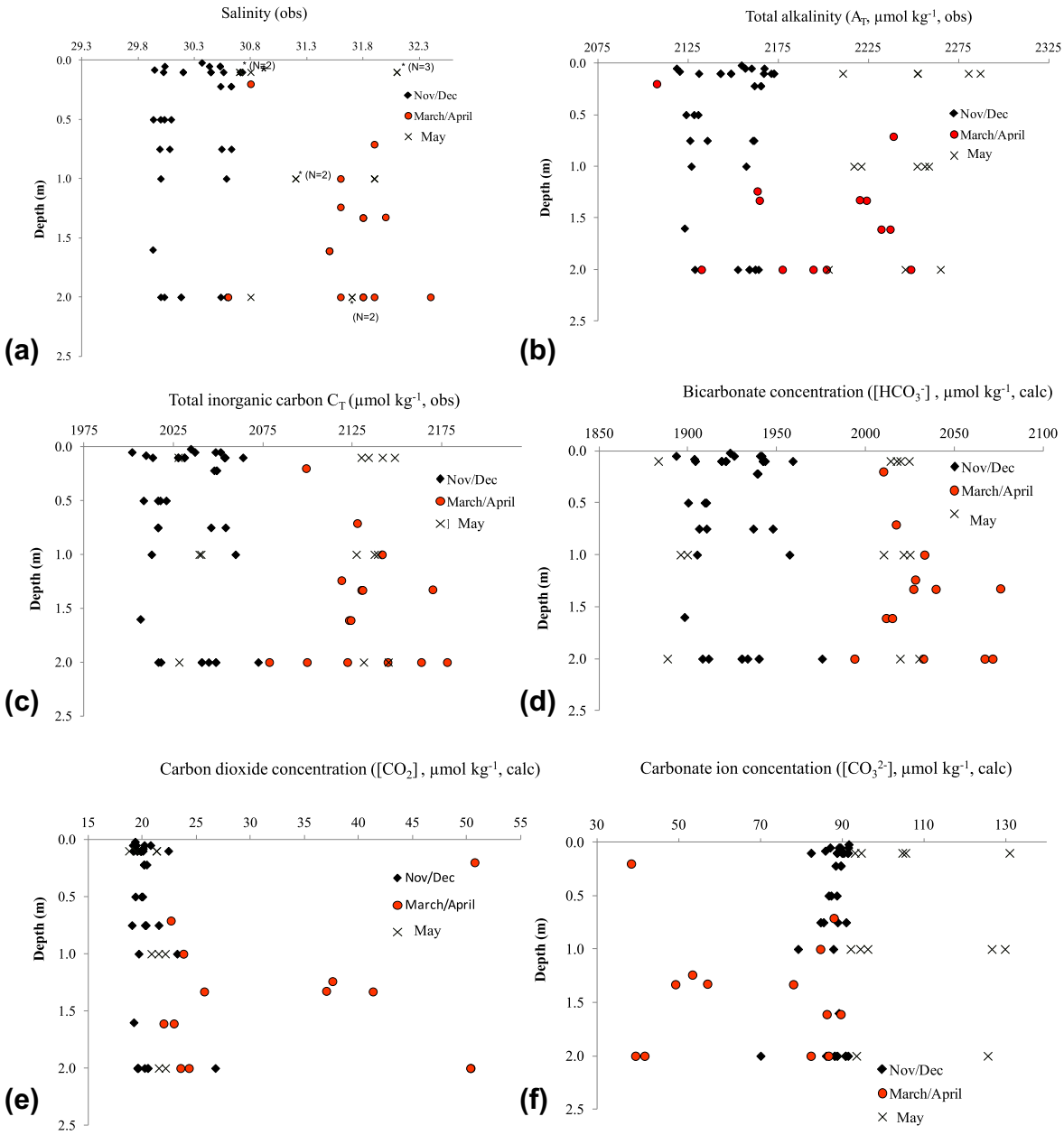

Figure 4. Evolution of under-ice water (UIW) (a) salinity, (b) total alkalinity (A_T, µmol kg^{-1}), (c) total inorganic carbon (C_T, µmol kg^{-1}), (d) bicarbonate ion concentration (HCO_3^-, µmol kg^{-1}), (e) carbon dioxide concentration (CO_2, µmol kg^{-1}, (f) carbonate ion concentration ([CO_3^{2-}], µmol kg^{-1}), (g) pH in situ, (h) pH at temperature 25°C (pH^{25}), (i) A_T:C_T ratio, (j) aragonite (ΩAr), and (k) calcite (ΩCa) for three periods; November/December, March/April, and May. "Obs" denotes that the values are measured and "calc" denotes that the values are calculated. Amount of overlapping points (N) are given for salinity.

December (Figure 4b). From March to May, the [CO_3^{2-}] increased from 40 µmol kg^{-1} to 130 µmol kg^{-1}, as the probable effect of dissolution of solid $CaCO_3$ during ice melt (Figure 4f). Assuming CO_2 uptake during primary production as a contributor to the increased [CO_3^{2-}], we used the [NO_3^-]:[CO_3^{2-}] ratio of 1:6 estimated by *Chierici et al.* [2011]. In our study, the change in [NO_3^-] (Table 2) corresponded to approximately 20 µmol kg^{-1} increase in [CO_3^{2-}], suggesting that 70 µmol kg^{-1} of the increase in the UIW was due to $CaCO_3$ precipitation. The $CaCO_3$ saturation level in UIW decreased from supersaturated ($\Omega > 1$) in November/December to March/April (Figures 4j and 4k). A likely explanation for the significantly reduced saturation states in March/April could be due to CO_2 release from the ice, consistent with the increased [CO_2] in the UIW (Figure 4e and Table 3). At this time, low ΩAr and ΩCa, and elevated pCO_2 and [CO_2] were also measured in the ice brines (Table 3). By the beginning of May, ΩAr and ΩCa increased to the maximum values of approximately 2.0 and 3.2 for ΩAr and ΩCa, respectively (Figures 4j and 4k). The

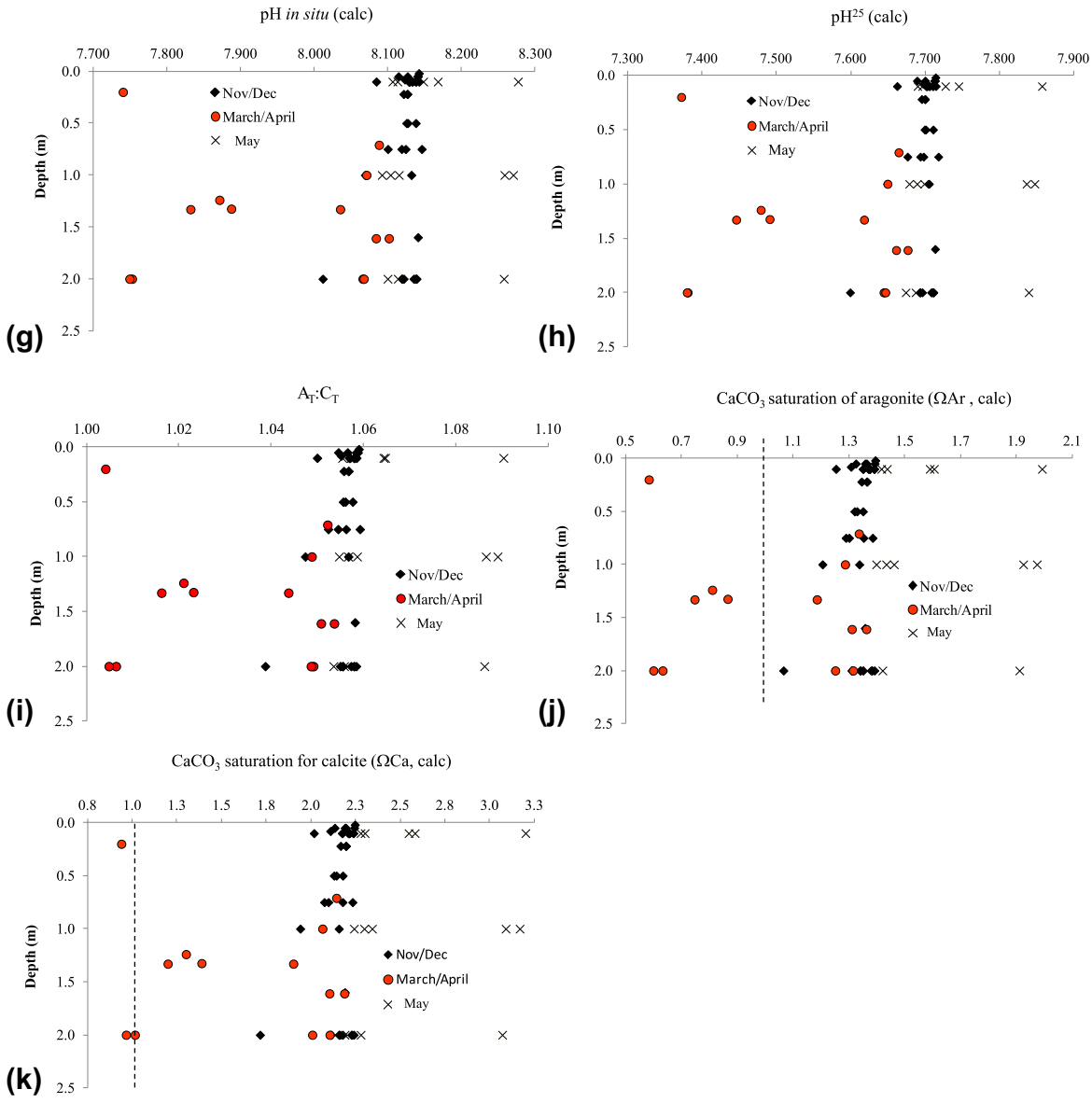

Figure 4. (continued)

increased Ω in the UIW in May (onset of ice melt) coincided with increased A_T and A_T:C_T ratio (Figures 4b and 4i). This implies that while sea-ice formation decreased Ω, the ice melt resulted in increased Ω. This increase was due to dissolution of solid $CaCO_3$, previously formed in the ice, both within draining ice brines and possibly within the water column after release from the ice.

[32] The results from our study partly contradict other studies in the Arctic Ocean showing that increased melt water results in low ΩAr levels [*Chierici and Fransson*, 2009; *Yamamoto-Kawai et al*., 2009]. These studies focused on the carbonate system in water depths below 10 m, while our study focused on the ice-water interface (upper 2 m). *Chierici et al*. [2011] found much smaller ΩAr seasonal variations of 0.3 and ΩCa of 0.5 over the upper 10 m than we found over the upper 2 m, which were 1.4 for ΩAr and 2.3 for ΩCa. It is also likely that the signal from the sea ice was quickly diluted and hence difficult to measure as it was mixed into the polar mixed layer (PML), described as the upper 60 m of the surface water [*Chierici et al*., 2011]. However, brine rejection during sea-ice formation is known to create a high-salinity winter layer, so-called upper halocline [*Rudels et al*., 1996]. Our study highlights the importance of the combined seasonal studies of the biogeochemistry in sea ice and underlying water, to understand the role of $CaCO_3$ precipitation and brine rejection for CO_2 uptake and the progress of ocean acidification.

4.3. Drivers of the Carbonate System in Sea Ice During Ice Formation

4.3.1. Approach and Calculations

[33] In Figure 5a, the linear fits between average sea-ice A_T and C_T and ice thickness for each ice core indicate that A_T and C_T were lost from the growing sea ice at approximately 1.9 μmol kg^{-1} and 1.8 μmol kg^{-1} cm^{-1} of ice thickness increase, respectively. The ice lost an average of approximately 0.011 μmol kg^{-1} d^{-1} of C_T and A_T over the 170 day ice formation period. To investigate the sea-ice C_T

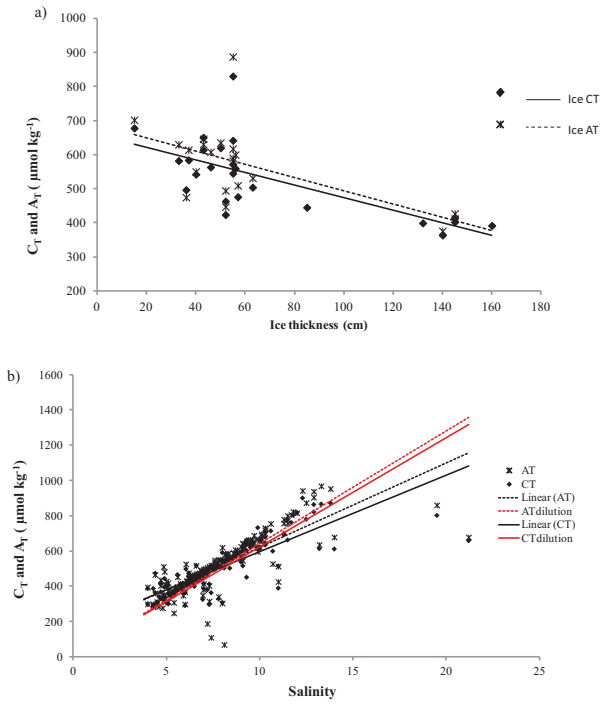

Figure 5. The linear fits between sea-ice A_T and C_T and (a) ice thickness (I_z), ($C_T = -1.8463 \times I_z + 658.57$, $R^2 = 0.48$, solid line); $A_T = -1.9416 \times I_z + 687.26$, $R^2 = 0.38$, dashed line) and (b) salinity ($C_T = 43.306 \times S + 162.46$, $R^2 = 0.70$, solid line; $A_T = 48.083 \times S + 139.23$, $R^2 = 0.63$, dashed line). The dilution lines (intercept = 0) for C_T ($CT_{DIL} = 62.182 \times S$, red solid line) and for A_T ($AT_{DIL} = 64.079 \times S$, red dashed line) are marked in red.

and A_T loss in more detail, we used the linear fits between all the sea-ice values of C_T and A_T and salinity for each full ice core, shown in Figure 5b. C_T and A_T concentrations should be proportional to salinity in sea ice, if the salinity change is due only to water balance [*Thomas et al*., 2010]. Deviations from the dilution line may be attributed to loss or gain of C_T and A_T by other processes, such as $CaCO_3$ precipitation/dissolution, biological processes, and CO_2 gas flux. The variability and impact of these processes on sea-ice C_T were investigated for each core and month, at all sections in the ice cores. We assumed that the sea ice was formed by the under-ice water (UIW) in November, and used the November mean values (C_0) at a salinity of 30.1, A_T of 2131 µmol kg^{-1} and C_T of 2016 µmol kg^{-1} (Table 3). The changes that were only explained by salinity changes (Cs) were compared to C_0 to estimate the impact due to other processes (ΔC, equation (4)), such as changes due to primary production (ΔC_{PP}), bacterial respiration (ΔC_{BR}), CO_2-gas flux (ΔC_{FCO2}) in or out of the ice, and $CaCO_3$ precipitation and dissolution (ΔC_{CaCO3}). The concentrations of C_T and A_T in the freezing seawater (i.e., UIW) were used as initial concentrations (C_0)

$$\Delta C = C_s - C_0 = \Delta C_{BR} + \Delta C_{PP} + \Delta C_{CaCO3} + \Delta C_{FCO2} \quad (4)$$

where the impact due to ΔC_{BR} is positive (gain) and ΔC_{PP} is negative (loss). Positive ΔC_{CaCO3} indicates precipitation (gain) and negative dissolution (loss), and positive ΔC_{FCO2} means gain and negative means loss.

[34] To estimate the effects of biological processes (ΔC_{BR} and ΔC_{PP}), we used results obtained by *Nguyen and Maranger* [2011] during the same expedition as our study. In sea ice, they estimated net heterotrophy between February and March and net autotrophy between April and mid-May. We used their bacterial respiration values of 23 µg C L^{-1} d^{-1} for November to March and 15 µg C L^{-1} d^{-1} for April and May integrated over 30 days, to correct for the C_T contribution of bacterial respiration (ΔC_{BR}). Since their study was focused at the bottom 10 cm of the ice core, these numbers were subtracted from the sea-ice C_T values at the bottom 10 cm section and 5 cm section of each ice core between March and May, and between November and December, respectively, to correct for the added CO_2 due to bacterial respiration. The BR-corrected C_T was salinity-corrected ($C_{Ts}(BR_{corr})$), to correct for the effect of water balance, which included all processes except bacterial respiration. Similar exercise was performed for the C_T consumption due to primary production. To the bottom ice sections, we added corresponding values of primary production (1.8 µg L^{-1} d^{-1} for November to March and 418 µg L^{-1} d^{-1} for April/mid-May) obtained from the results for February to May by *Nguyen and Maranger* [2011], where they compared the measured respiration estimates with previously reported rates of primary production from the same region. Therefore, the salinity-corrected and PP-corrected values ($C_{Ts}(PP_{corr})$) include all processes except primary production and salinity effect. We calculated ΔC_{BR} and ΔC_{PP} from the difference between C_0 and C_{Ts}(BRcorr) and C_{Ts}(PPcorr), which were compared to ΔC_T, according to:

$$\Delta C_{BR} = \Delta C_T - (C_{Ts}(BR_{corr}) - C_0) \quad (5)$$

$$\Delta C_{PP} = \Delta C_T - (C_{Ts}(PP_{corr}) - C_0) \quad (6)$$

[35] The A_T change, estimated from the difference between ΔA_{Ts} (salinity-corrected) and A_{T0} can be mainly explained by $CaCO_3$ precipitation in the sea ice since ΔC_{PP} and ΔC_{BR} are assumed to have insignificant impacts on A_T. If the solid $CaCO_3$ escapes from the ice, either to the underlying water or to the ice surface with upwardly flowing brine, to form brine skims and/or frost flowers, both A_T and C_T would decrease roughly in proportion to salinity. However, if $CaCO_3$ precipitates and remains within the ice, bulk-ice samples would be enriched in A_T relative to C_T and salinity [*Rysgaard et al*., 2013]. In some cases, A_T could be lost in relation to salinity when solid $CaCO_3$ is lost at ice extraction. We used the theoretical change in the A_T:C_T molar ratio of 2 for $CaCO_3$ precipitation within the ice to estimate its potential effect on bulk-ice C_T (equation (7)):

$$\Delta C_{CaCO3} = (A_{Ts} - A_{T0})/2 \quad (7)$$

[36] The CO_2 gas fluxes (ΔC_{FCO2}) were estimated by the difference between the change in C_T (ΔC_T) and the changes attributed to primary production, bacterial respiration, and $CaCO_3$ precipitation, according to equation (8), and are summarized in Table 4a and Table 4b.

Table 4a. Estimates of Salinity-Corrected C_T (Cs), and the Change in C_T Due to Sea-Ice Processes (ΔC_T), the Contribution of $CaCO_3$ Precipitation and Dissolution ($\Delta C_T(CaCO_3)$), Primary Production ($\Delta C_T(PP)$), Bacterial Respiration ($\Delta C_T(BR)$), and CO_2-Gas Flux ($\Delta C_T(FCO_2)$) (All in μmol kg^{-1}) in Bulk Sea Ice, Together With Sampling Dates, Days and Ice Sections (cm)[a]

Date	Ice Section	Days	CTs	ΔCT	CV (%) ΔCT	ΔCT ($CaCO_3$)	CV (%) ΔCT ($CaCO_3$)	ΔCT (BR)	CV (%) ΔCT (BR)	ΔCT (PP)	CV (%) ΔCT (PP)	ΔCT (FCO_2)	CV (%) ΔCT (FCO_2)
19 Nov	2.5	51	1917	−99	3	−11	25	n.a.	n.a.	n.a.	n.a.	−88	5
19 Nov	7.5	51	1990	−26	11	−7	42	n.a.	n.a.	n.a.	n.a.	−20	20
19 Nov	12.5	51	1958	−58	5	−18	15	n.a.	n.a.	n.a.	n.a.	−39	10
19 Nov	20.5	51	1976	−40	7	−3	86	n.a.	n.a.	n.a.	n.a.	−37	11
19 Nov	28.5	51	1957	−59	5	−7	38	n.a.	n.a.	n.a.	n.a.	−51	8
19 Nov	36.5	51	1934	−82	3	−26	11	n.a.	n.a.	n.a.	n.a.	−56	7
19 Nov	44.5	51	1942	−74	4	−18	16	217	7	−7	N.S.	−266	6
22 Nov	2.5	62	1900	−116	2	−27	11	n.a.	n.a.	n.a.	n.a.	−90	4
22 Nov	7.5	62	2010	−6	49	2	N.S.	n.a.	n.a.	n.a.	n.a.	−7	53
22 Nov	12.5	62	1965	−51	6	−25	11	n.a.	n.a.	n.a.	n.a.	−25	16
22 Nov	20.0	62	1949	−67	4	−29	10	n.a.	n.a.	n.a.	n.a.	−38	10
22 Nov	30.0	62	1959	−57	5	−22	13	n.a.	n.a.	n.a.	n.a.	−36	11
22 Nov	37.5	62	1948	−68	4	−22	13	n.a.	n.a.	n.a.	n.a.	−46	9
22 Nov	42.4	62	1957	−59	5	−17	17	n.a.	n.a.	n.a.	n.a.	−42	9
22 Nov	47.5	62	1957	−59	5	−20	14	n.a.	n.a.	n.a.	n.a.	−39	10
22 Nov	52.5	62	2002	−14	20	18	16	226	7	−8	N.S.	−249	6
28 Nov	2.5	58	1864	−152	2	−29	10	n.a.	n.a.	n.a.	n.a.	−123	3
28 Nov	7.5	59	2005	−11	27	−14	20	n.a.	n.a.	n.a.	n.a.	3	N.S.
28 Nov	12.5	60	1933	−83	3	−47	6	n.a.	n.a.	n.a.	n.a.	−36	11
28 Nov	30	61	2005	−11	26	−12	23	n.a.	n.a.	n.a.	n.a.	1	N.S.
28 Nov	45	62	1994	−22	13	−5	55	n.a.	n.a.	n.a.	n.a.	−17	23
28 Nov	50	63	2029	13	22	0.03	N.S.	306	5	−11	N.S.	−283	6
2 Dec	2.5	37	1877	−139	2	−15	19	n.a.	n.a.	n.a.	n.a.	−124	3
2 Dec	7.5	37	1996	−20	14	−6	48	n.a.	n.a.	n.a.	n.a.	−14	28
2 Dec	12.5	37	1990	−26	11	−3	N.S.	n.a.	n.a.	n.a.	n.a.	−24	17
2 Dec	17.5	37	1991	−25	11	8	34	n.a.	n.a.	n.a.	n.a.	−33	12
2 Dec	32	37	1920	−96	3	−42	7	175	9	−6	N.S.	−223	7
6 Dec	2.5	41	1956	−60	5	−30	9	n.a.	n.a.	n.a.	n.a.	−29	14
6 Dec	7.5	41	1982	−34	8	−17	16	n.a.	n.a.	n.a.	n.a.	−16	24
6 Dec	12.5	41	2009	−7	43	−18	16	n.a.	n.a.	n.a.	n.a.	11	36
6 Dec	30	41	1987	−29	10	−20	14	n.a.	n.a.	n.a.	n.a.	−9	46
6 Dec	34	41	1988	−28	10	−33	9	195	195	−7	N.S.	−184	9
12 Dec	2.5	63	1852	−164	2	−1	N.S.	n.a.	n.a.	n.a.	n.a.	−163	2
12 Dec	7.5	63	1952	−64	4	−39	7	n.a.	n.a.	n.a.	n.a.	−25	16
12 Dec	12.5	63	1980	−36	8	−25	11	n.a.	n.a.	n.a.	n.a.	−11	36
12 Dec	20	63	1985	−31	9	−29	10	n.a.	n.a.	n.a.	n.a.	−2	N.S.
12 Dec	30	63	1996	−20	14	−16	18	n.a.	n.a.	n.a.	n.a.	−4	N.S.
12 Dec	40	63	1976	−40	7	−27	10	n.a.	n.a.	n.a.	n.a.	−13	31
12 Dec	50	63	1956	−60	5	−22	12	n.a.	n.a.	n.a.	n.a.	−37	11
12 Dec	55	63	1983	−33	8	−4	67	281	281	−10	N.S.	−300	5
14 Dec	2.5	70	1843	−173	2	−58	5	n.a.	n.a.	n.a.	n.a.	−115	3
14 Dec	7.5	70	1985	−31	9	−26	11	n.a.	n.a.	n.a.	n.a.	−4	93
14 Dec	12.5	70	1979	−37	8	−38	7	n.a.	n.a.	n.a.	n.a.	1	N.S.
14 Dec	20	70	2009	−7	41	−20	14	n.a.	n.a.	n.a.	n.a.	13	30
14 Dec	30	70	2030	14	20	−9	31	n.a.	n.a.	n.a.	n.a.	23	17
14 Dec	40	70	2026	10	27	−17	16	n.a.	n.a.	n.a.	n.a.	28	14
14 Dec	52	70	1992	−24	12	−20	14	n.a.	n.a.	n.a.	n.a.	−4	92
14 Dec	60	70	1988	−28	10	−5	52	220	220	−8	N.S.	−234	7
25 Mar	10	161	1636	−380	1	−190	1	n.a.	n.a.	n.a.	n.a.	−190	2
25 Mar	20	161	1854	−162	2	−139	2	n.a.	n.a.	n.a.	n.a.	−23	18
25 Mar	30	161	1972	−44	6	−108	3	n.a.	n.a.	n.a.	n.a.	64	6
25 Mar	40	161	2376	360	1	100	3	n.a.	n.a.	n.a.	n.a.	260	2
25 Mar	50	161	2749	733	0.4	282	1	n.a.	n.a.	n.a.	n.a.	452	1
25 Mar	60	161	2153	137	2	502	1	n.a.	n.a.	n.a.	n.a.	−365	1
25 Mar	80	161	2291	275	1	−47	6	n.a.	n.a.	n.a.	n.a.	323	1
25 Mar	100	161	1945	−71	4	−108	3	n.a.	n.a.	n.a.	n.a.	37	11
25 Mar	110	161	1912	−104	3	−126	2	n.a.	n.a.	n.a.	n.a.	22	18
25 Mar	120	161	1732	−284	1	−162	2	n.a.	n.a.	n.a.	n.a.	−123	3
25 Mar	130	161	1812	−204	1	−174	2	n.a.	n.a.	n.a.	n.a.	−30	13

Table 4a. (continued)

Date	Ice Section	Days	CTs	ΔCT	CV (%) ΔCT	ΔCT ($CaCO_3$)	CV (%) ΔCT ($CaCO_3$)	ΔCT (BR)	CV (%) ΔCT (BR)	ΔCT (PP)	CV (%) ΔCT (PP)	ΔCT (FCO_2)	CV (%) ΔCT (FCO_2)
25 Mar	140	161	2757	741	0.4	278	1	381	381	−13	N.S.	95	17
28 Mar	7.5	161	1484	−532	0.5	−278	1	n.a.	n.a.	n.a.	n.a.	−254	2
28 Mar	22.5	161	1453	−563	0.5	−346	1	n.a.	n.a.	n.a.	n.a.	−217	2
28 Mar	42.5	161	1901	−115	2	−45	6	n.a.	n.a.	n.a.	n.a.	−70	6
28 Mar	57.5	161	2669	653	0.4	386	1	n.a.	n.a.	n.a.	n.a.	266	2
28 Mar	77.5	161	2564	548	0.5	271	1	n.a.	n.a.	n.a.	n.a.	277	1
28 Mar	94.5	161	2479	463	0.6	196	1	n.a.	n.a.	n.a.	n.a.	267	2
28 Mar	109.5	161	2878	862	0.3	360	1	n.a.	n.a.	n.a.	n.a.	502	1
28 Mar	126.5	161	2019	3	105	−46	6	n.a.	n.a.	n.a.	n.a.	49	8
28 Mar	143.5	161	2838	822	0.3	349	1	390	4	−14	N.S.	97	17
31 Mar	7.5	156	937	−1079	0.3	−554	1	n.a.	n.a.	n.a.	n.a.	−526	1
31 Mar	22.5	156	1382	−634	0.4	−384	1	n.a.	n.a.	n.a.	n.a.	−249	2
31 Mar	37.5	156	1220	−796	0.4	−418	1	n.a.	n.a.	n.a.	n.a.	−378	1
31 Mar	55.5	156	1969	−47	6	n.d.	n.d.	n.d.	n.a.	n.d.	n.a.	n.d.	n.d.
31 Mar	72.5	156	1520	−496	0.6	−278	1	n.a.	n.a.	n.a.	n.a.	−217	2
31 Mar	89.5	156	1712	−304	0.9	−184	2	n.a.	n.a.	n.a.	n.a.	−119	3
31 Mar	106.5	156	3184	1168	0.2	615	0.5	n.a.	n.a.	n.a.	n.a.	553	1
31 Mar	116.5	156	2106	90	3	8	35	n.a.	n.a.	n.a.	n.a.	82	5
31 Mar	136.5	156	1881	−135	2	−59	5	330	5	−12	N.S.	−395	4
31 Mar	5.5	61	1419	−597	0.5	−304	1	n.a.	n.a.	n.a.	n.a.	−293	1
31 Mar	17.5	61	1939	−77	4	−104	3	n.a.	n.a.	n.a.	n.a.	27	15
31 Mar	28.5	61	1408	−608	0.5	−365	1	n.a.	n.a.	n.a.	n.a.	−244	2
31 Mar	38.5	61	2105	89	3	−37	7	n.a.	n.a.	n.a.	n.a.	127	3
31 Mar	53.5	61	3327	1311	0.2	659	0.4	429	3	−15	100	239	7
2 May	7.5	94	1685	−331	0.8	−325	1	n.a.	n.a.	n.a.	n.a.	−6	65
2 May	42.5	94	1588	−428	0.7	−674	0.4	n.a.	n.a.	n.a.	n.a.	246	2
2 May	74.5	94	2104	88	3	39	7	78	19	−2177	1	2148	1
6 May	8	89	1892	−124	2	−158	2	n.a.	n.a.	n.a.	n.a.	34	12
6 May	38	89	2320	304	1	112	3	n.a.	n.a.	n.a.	n.a.	192	2
6 May	68	89	2459	443	1	469	1	106	14	−2953	1	2821	1

[a]The relative standard deviation (CV, %) is the cumulative error of the analytical error for each parameter. Not significant values are denoted N.S., n.d. for no data, and n.a. denotes not applicable data.

$$\Delta C_{FCO2} = \Delta C_T - (\Delta C_{BR} + \Delta C_{PP} + \Delta C_{CaCO3}) \quad (8)$$

4.3.2. C_T Change Due to Sea-Ice Processes

[37] The changes of C_T due to sea-ice processes showed large variability both within the ice core and between months (Tables 4a and 4b). Both positive and negative ΔC_{CaCO3} indicate that C_T was affected by $CaCO_3$ precipitation, estimated from larger A_T changes in relation to salinity. Positive ΔC_{FCO2} indicates a C_T gain due to CO_2 uptake from surrounding environment, and negative corresponds to a C_T loss. Large C_T gradients and variability in processes were observed, in particular between the interfaces and the midpart of the ice cores (Table 4a). Figure 6 summarizes the changes at the ice-snow/air interface (top ice), transition (midice), and at the ice-water interface (bottom ice). The top ice was mainly affected by a C_T loss between 300 and 500 μmol kg^{-1} (March to May) and between 10 and 50 μmol kg^{-1} (November to December) due to $CaCO_3$ dissolution and/or A_T and $CaCO_3$ loss through frost flowers. The C_T loss was also due to CO_2-gas flux (CO_2 outgassing), where CO_2 may have escaped to the atmosphere through the brine skim. From March to May 2008, these processes were more significant in all sections, compared to from November to December 2007 (Figures 6a and 6b). The midice had large variability, in both ΔC_{CaCO3} and ΔC_{FCO2}, with both C_T loss and gain, particularly between March and May (Figures 6c and 6d). From November to December, <20 μmol kg^{-1} and 40 μmol kg^{-1} C_T loss were estimated, as an effect of $CaCO_3$ dissolution and CO_2 outgassing, respectively. The bottom ice was highly dynamic at all ice cores during all months (Figures 6e and 6f). Bacterial respiration was important from November to December and in March with a CO_2 gain between 200 and 400 μmol kg^{-1} (Figures 6e and 6f). Primary production was the most significant process at the bottom ice in May, with a C_T loss larger than 2000 μmol kg^{-1}, which was compensated by CO_2 uptake (gain) from the atmosphere and underlying water. The effect of $CaCO_3$ precipitation and dissolution at the bottom ice was mostly pronounced in March and May with estimates between 300 and 600 μmol kg^{-1}, also affecting the CO_2 flux. This result coincides with the elevated A_T, high A_T:C_T and A_T:S in brine in March (Table 3), suggesting precipitation of $CaCO_3$. Compared to a recent study in Arctic sea ice, *Rysgaard et al*. [2013] estimated ikaite concentrations in nonmelted sea ice of 100–200 μmol kg^{-1} at the ice-water interface (bottom ice), and

Table 4b. Daily Estimates (μmol kg^{-1} d^{-1}) of Each Sea-Ice Process (Table 4a) Are Derived From Numbers of Days Since Ice Formation (Days), Based on the Ice Thickness (Table 1) and Daily Rate of 0.9 cm d^{-1} (160 cm/170 days) Ice Growth and the Estimates of C_T Change

Date	Ice Section	Days	Daily ΔCT ($CaCO_3$)	Daily ΔCT (BR)	Daily ΔCT (PP)	Daily ΔCT (FCO_2)
19 Nov	2.5	51	−0.2	n.a.	n.a.	−2
19 Nov	7.5	51	−0.1	n.a.	n.a.	−0.4
19 Nov	12.5	51	−0.4	n.a.	n.a.	−1
19 Nov	20.5	51	−0.1	n.a.	n.a.	−1
19 Nov	28.5	51	−0.1	n.a.	n.a.	−1
19 Nov	36.5	51	−0.5	n.a.	n.a.	−1
19 Nov	44.5	51	−0.3	4	−0.1	−5
22 Nov	2.5	62	−0.4	n.a.	n.a.	−1
22 Nov	7.5	62	<0.1	n.a.	n.a.	−0.1
22 Nov	12.5	62	−0.4	n.a.	n.a.	−0.4
22 Nov	20.0	62	−0.5	n.a.	n.a.	−1
22 Nov	30.0	62	−0.3	n.a.	n.a.	−1
22 Nov	37.5	62	−0.3	n.a.	n.a.	−1
22 Nov	42.4	62	−0.3	n.a.	n.a.	−1
22 Nov	47.5	62	−0.3	n.a.	n.a.	−1
22 Nov	52.5	62	0.3	4	−0.1	−4
28 Nov	2.5	58	−0.5	n.a.	n.a.	−2
28 Nov	7.5	59	−0.2	n.a.	n.a.	0.1
28 Nov	12.5	60	−0.8	n.a.	n.a.	−1
28 Nov	30	61	−0.2	n.a.	n.a.	<0.1
28 Nov	45	62	−0.1	n.a.	n.a.	−0.3
28 Nov	50	63	<0.1	5	−0.2	−4
2 Dec	2.5	37	−0.4	n.a.	n.a.	−3
2 Dec	7.5	37	−0.2	n.a.	n.a.	−0.4
2 Dec	12.5	37	−0.1	n.a.	n.a.	−1
2 Dec	17.5	37	0.2	n.a.	n.a.	−1
2 Dec	32	37	−1.2	5	−0.2	−6
6 Dec	2.5	41	−0.7	n.a.	n.a.	−1
6 Dec	7.5	41	−0.4	n.a.	n.a.	−0.4
6 Dec	12.5	41	−0.4	n.a.	n.a.	0.3
6 Dec	30	41	−0.5	n.a.	n.a.	−0.2
6 Dec	34	41	−0.8	5	−0.2	−4
12 Dec	2.5	63	< −0.1	n.a.	n.a.	−3
12 Dec	7.5	63	−0.6	n.a.	n.a.	−0.4
12 Dec	12.5	63	−0.4	n.a.	n.a.	−0.2
12 Dec	20	63	−0.5	n.a.	n.a.	< −0.1
12 Dec	30	63	−0.3	n.a.	n.a.	−0.1
12 Dec	40	63	−0.4	n.a.	n.a.	−0.2
12 Dec	50	63	−0.4	n.a.	n.a.	−1
12 Dec	55	63	−0.1	4	−0.2	−5
14 Dec	2.5	70	−0.8	n.a.	n.a.	−2
14 Dec	7.5	70	−0.4	n.a.	n.a.	−0.1
14 Dec	12.5	70	−0.5	n.a.	n.a.	<0.1
14 Dec	20	70	−0.3	n.a.	n.a.	0.2
14 Dec	30	70	−0.1	n.a.	n.a.	0.3
14 Dec	40	70	−0.2	n.a.	n.a.	0.4
14 Dec	52	70	−0.3	n.a.	n.a.	−0.1
14 Dec	60	70	−0.1	3	−0.1	−3
25 Mar	10	161	−1	n.a.	n.a.	−1
25 Mar	20	161	−0.9	n.a.	n.a.	−0.1
25 Mar	30	161	−0.7	n.a.	n.a.	0.4
25 Mar	40	161	0.6	n.a.	n.a.	2
25 Mar	50	161	2	n.a.	n.a.	3
25 Mar	60	161	3	n.a.	n.a.	−2
25 Mar	80	161	−0.3	n.a.	n.a.	2
25 Mar	100	161	−0.7	n.a.	n.a.	0.2
25 Mar	110	161	−0.8	n.a.	n.a.	0.1
25 Mar	120	161	−1	n.a.	n.a.	−1
25 Mar	130	161	−1	n.a.	n.a.	−0.2
25 Mar	140	161	2	2	−0.1	1
28 Mar	7.5	161	−2	n.a.	n.a.	−2

Table 4b. (continued)

Date	Ice Section	Days	Daily ΔCT ($CaCO_3$)	Daily ΔCT (BR)	Daily ΔCT (PP)	Daily ΔCT (FCO_2)
28 Mar	22.5	161	−2	n.a.	n.a.	−1
28 Mar	42.5	161	−0.3	n.a.	n.a.	−0.4
28 Mar	57.5	161	2	n.a.	n.a.	2
28 Mar	77.5	161	2	n.a.	n.a.	2
28 Mar	94.5	161	1	n.a.	n.a.	2
28 Mar	109.5	161	2	n.a.	n.a.	3
28 Mar	126.5	161	−0.3	n.a.	n.a.	0.3
28 Mar	143.5	161	2	2	−0.1	1
31 Mar	7.5	156	−4	n.a.	n.a.	−3
31 Mar	22.5	156	−2	n.a.	n.a.	−2
31 Mar	37.5	156	−3	n.a.	n.a.	−2
31 Mar	55.5	156	n.d.	n.d.	n.d.	n.d.
31 Mar	72.5	156	−2	n.a.	n.a.	−1
31 Mar	89.5	156	−1	n.a.	n.a.	−1
31 Mar	106.5	156	4	n.a.	n.a.	4
31 Mar	116.5	156	0.1	n.a.	n.a.	1
31 Mar	136.5	156	−0.4	2	−0.1	−3
31 Mar	5.5	61	−5	n.a.	n.a.	−5
31 Mar	17.5	61	−2	n.a.	n.a.	0.4
31 Mar	28.5	61	−6	n.a.	n.a.	−4
31 Mar	38.5	61	−0.6	n.a.	n.a.	2
31 Mar	53.5	61	11	7	−0.2	4
2 May	7.5	94	−3	n.a.	n.a.	−0.1
2 May	42.5	94	−7	n.a.	n.a.	3
2 May	74.5	94	0.4	0.8	−23	23
6 May	8	89	−2	n.a.	n.a.	0.4
6 May	38	89	1	n.a.	n.a.	2
6 May	68	89	5	1	−33	32

700–900 μmol kg^{-1} at the ice-air interface (top ice), thus our estimates agree well with their study. The loss of C_T due to CO_2 flux in our study was important in November and December at the bottom due to brine rejection and addition of CO_2 at bacterial respiration. In May, the CO_2 flux was the largest with a CO_2 gain of >2000 μmol kg^{-1}, mainly as a result of the C_T loss at primary production.

[38] Figure 7 summarizes the relative importance (%) with the uncertainty (error bars) due to the variability between cores and analytical error of each process (except salinity change), to the total C_T change in the top ice, midsection and bottom ice (in connection to water) from November to December 2007 and March to May 2008, including the ice cores in Table 4a. The largest relative importance was due to CO_2 fluxes in most sections and months, with the largest relative CO_2 flux of approximately 80% at the top ice between November and December (Figure 7). The largest relative effect (60%) was due to $CaCO_3$ at the top and midice between March and May.

[39] In ice cores where the temperatures at the top of the ice were warmer than −10°C (Figure 2d), the potential for CO_2-gas flux (outgassing; Figures 6a and 6b) increased, in accordance to the CO_2-flux studies of *Nomura et al*. [2006] and *Geilfus et al*. [2012, 2013]. We also observed a thin layer of snow on top of the ice, but no superimposed ice. According to *Albert et al*. [2002] snow has high permeability and could allow gas exchange between ice and atmosphere, depending on wind speed.

4.3.3. Uncertainty of the Process Estimates

[40] In the calculations of the drivers, the uncertainties of the estimated impact of sea-ice processes on C_T were investigated and are shown as the relative standard deviation (CV, %) in Table 4a. These uncertainties were calculated as the cumulative variability due to the analytical errors in each parameter (C_T or A_T) used in the calculations of the impact for each process. Since the CO_2-gas flux estimates are the residual of the measured ΔC_T minus the contributions by the bacterial respiration, primary production and $CaCO_3$ precipitation, the largest accumulated uncertainties were calculated. *Nguyen and Maranger* [2011] reported 20% uncertainty in their estimates of BR and PP. The cumulative uncertainty for the resulting CO_2-gas flux was 16 μmol kg^{-1} between November and March, and 26 μmol kg^{-1} in May. For the ice sections in the midparts, no primary production and bacterial respiration were estimated, resulting in the cumulative uncertainty of 4 μmol kg^{-1} in the CO_2 gas flux estimates. From November to March, the impact of primary production was insignificant resulting in insignificant uncertainty. We assumed that bacterial respiration was significant in the bottom ice during all months, with a determination uncertainty of 15 μmol kg^{-1}. For the estimates of the CO_2-gas flux, most of the values were significant, except for a few values in the midparts of the ice cores in November (Table 4a). In general, between March and May the relative standard deviation was lower in the midparts of the ice cores than from November to December, (Table 4a). For all ice cores, the ice-air interface (top) showed the most significant values on the CO_2-gas flux estimates, with CV varying between 1% and 14%, except for in May where CV was higher. At the ice-water interface (bottom), CV varied between 1% and 17% including all ice cores, with the lowest CV of 1% in May (Table 4a). All ice cores had lower relative standard deviation at the ice-air interface (top) and ice-water

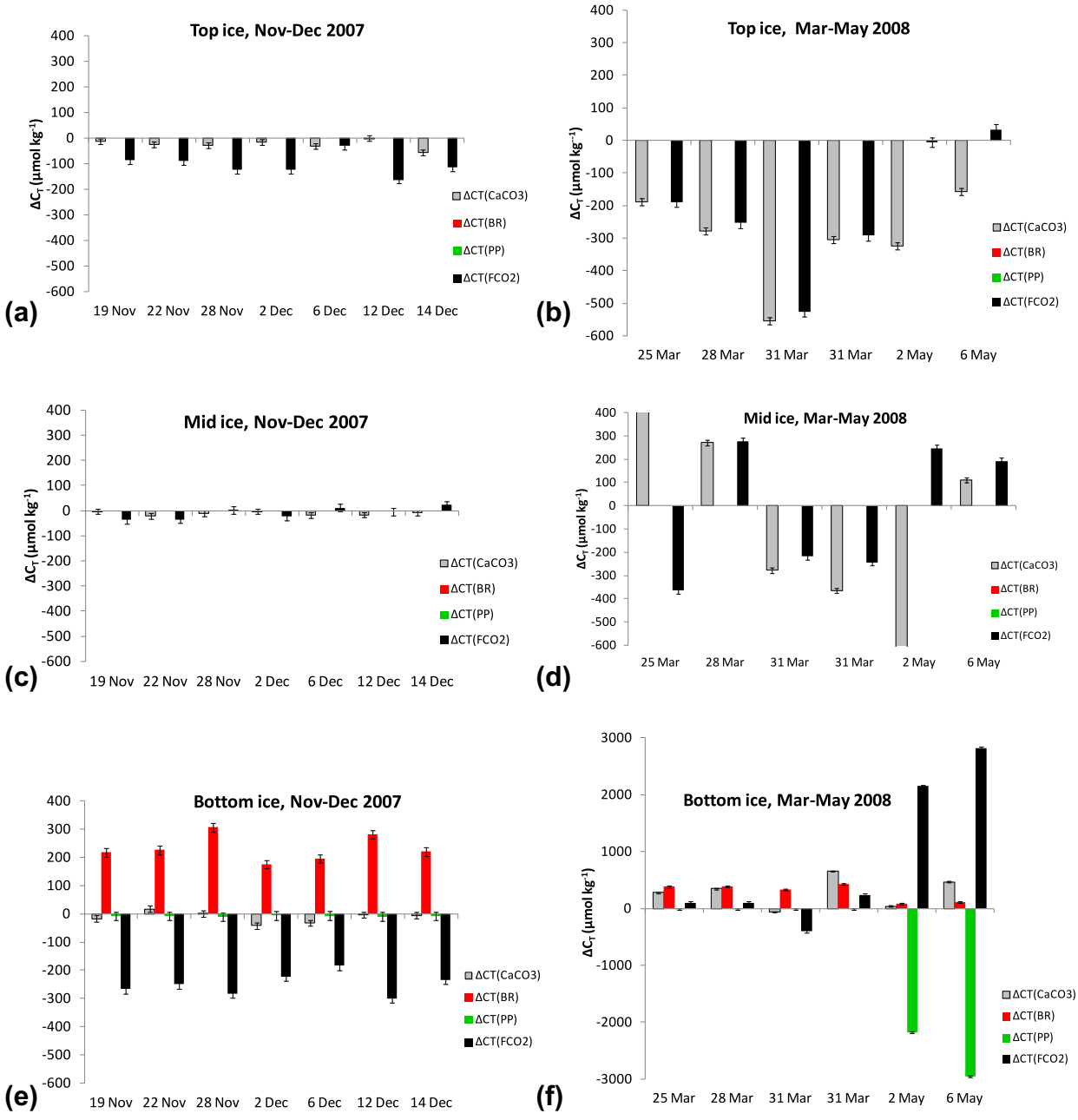

Figure 6. The impact of sea-ice processes on ΔC_T since ice formation due to calcium carbonate precipitation and dissolution (ΔC_{TCaCO3}: gray), bacterial respiration (ΔC_{TBR}: red), primary production (ΔC_{TPP}: green), and CO_2-gas flux (ΔC_{TFCO2}: black), collected at (a) top ice between November and December 2007, (b) top ice between March and May 2008, (c) midice between November and December 2007, (d) midice between March and May, (e) bottom ice between November and December 2007, and (f) bottom ice between March and May (note that the scale is larger than the other scales). Error bars are the cumulative uncertainty in the estimated processes due to the analytical error and the variability in C_0.

interface (bottom) compared to the midparts, suggesting higher certainty in the estimates of the impact of the processes at the interfaces. This was mainly due to the larger C_T changes and impact of the processes at the interfaces compared to in the midparts. Between March and May, the CV was lower for $CaCO_3$ precipitation and CO_2 gas flux than between November and December, suggesting that the older and thicker ice was more impacted by $CaCO_3$ precipitation and CO_2-gas flux.

[41] In the approach of the driver estimates, we used C_0 as the starting values of the UIW in November. However, there is a natural variability in C_0 values in November (Table 3). The cumulative uncertainty of the variability in C_0 and the analytical errors are shown as error bars in Figure 6. The cumulative uncertainty of both the analytical errors of the parameters (C_0 of C_T by ± 9 μmol kg^{-1} and A_T by ± 11 μmol kg^{-1}, Table 3) and the variability in C_0 values showed that the CO_2-gas flux changed the most in

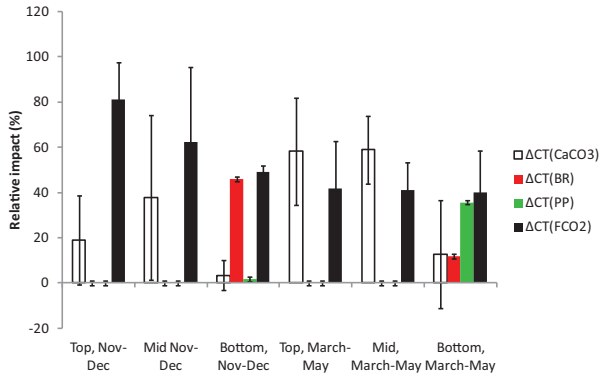

Figure 7. The relative importance (%) and the cumulative uncertainty (error bars) due to natural variability between the ice cores and analytical error in the estimates of calcium carbonate precipitation/dissolution (ΔC_{TCaCO3}; gray), bacterial respiration (ΔC_{TBR}; red), primary production (ΔC_{TPP}; green), and CO_2 fluxes (ΔC_{TFCO2}; black) to the total C_T change. The relative changes are averaged over the top ice, midice, and bottom ice in cores presented in Table 4a, collected from November to December 2007 and from March to May 2008, respectively.

November and December, with nonsignificant values (CV > 100%) in the midparts of the ice cores (not shown). At the ice-water interface, the CV changed between 0% and 5% for all ice cores due to the addition of the C_0 uncertainty. At the ice-air interface the CV changed up to 37% (in November), with less CV change from December to May. In Figure 7, the relative importance of each process and the error bars are a composite of the variability between the ice cores, analytical error and variability in C_0. However, the large uncertainty is mainly due to the variability between the ice samples, suggesting that the natural variability between ice cores is significantly larger than the uncertainties in analytical methods and calculations, which can be distinguished from the presentation of each ice core in Figure 6.

[42] In the calculations of the impact on C_T due to primary production, we assumed the primary production to occur only at the bottom of the ice, as suggested by *Horner and Schrader* [1982] and *Hsiao et al*. [1992]. In winter, primary production in the Arctic has shown to be insignificant but small. *Hsiao et al*. [1992] found active cells of ice algae in Arctic winter ice. Our estimates in fall/winter ice in November and December were an assumption that primary production was the same values as estimated in February [*Nguyen and Maranger*, 2011] since we had no estimates in November to December. The primary production may have been overestimated during this period. However, the PP values were relatively small, resulting in an insignificant effect on C_T. In our approach, bacterial respiration was estimated for the whole study period. However, from November to December there were no estimates of bacterial respiration. We assumed that bacterial respiration in bottom ice was the same in November and December as in March. This approximation may have resulted in overestimation of the impact on C_T by bacterial respiration. However, if we assume that bacterial respiration occurred in the entire ice core during the study period, this would result in more negative CO_2-gas flux (C_T loss) or less positive flux. In addition, the effect of solid $CaCO_3$ may be underestimated due to the loss of $CaCO_3$, A_T and brine at ice-core extraction.

4.3.4. Ice-Air CO_2 Exchange Through Frost Flowers

[43] The CO_2 depletion in the melted frost flowers (Table 3) was likely due to the evasion of CO_2 into the atmosphere, from the previously CO_2-rich frost flowers, as the effect of $CaCO_3$ precipitation. The A_T:C_T ratios in our melted frost flower were higher than in the sea-ice brines at some sampling sites (Table 3), implying $CaCO_3$ precipitation and CO_2 loss [e.g., *Rysgaard et al*., 2007] at the ice surface.

[44] We estimated the amount of CO_2 lost (C_{Tout}) from the brine (assuming linearity between C_T and salinity) to the atmosphere through frost flowers or brine skim in March (Table 3), using the mean brine C_T (C_{Tbrine}) of 7178 μmol kg^{-1}, brine salinity (S_{brine}) of 134, and frost-flower salinity (S_{FF}) of 48. We calculated the C_T of frost flowers (C_{Tcalc}), using the linear relation between S_{FF} and S_{brine}, multiplied with C_{Tbrine} (equation (9)). C_{Tcalc} was compared to the measured C_T in frost flowers (C_{TFF}; 2503 μmol kg^{-1}) in March, equation (10):

$$C_{Tcalc} = S_{FF} / S_{brine} * C_{Tbrine} \quad (9)$$

$$C_{Tout} = C_{Tcalc} - C_{TFF} \quad (10)$$

[45] The value of C_{Tcalc} was 2571 μmol kg^{-1}, which suggests that 68 μmol kg^{-1} was lost to the atmosphere, which was less than the CO_2 loss (200–500 μmol kg^{-1}) obtained from the process study (Figure 6b and Table 4a). The loss by the background wetted ice is unaccounted for, but represents a conduit for sea-ice CO_2 loss to the atmosphere whenever the brine is in a state of supersaturation.

Table 5. Average Values of Total Alkalinity (A_T), Total Inorganic Carbon (C_T), fCO_2 and Salinity in the Under-Ice Water (UIW; Upper 2 m), Upper Mixed Layer of 20 m (UML_{20}), and Winter Sea Ice in End of March/April (Before Onset of Melt in May), Representing the Properties of Ice Melt[a]

Type		S	A_T (μmol kg^{-1})	C_T (μmol kg^{-1})	pH in Situ	fCO_2 (μatm)	$[HCO_3^-]$ (μmol kg^{-1})	$[CO_3^{2-}]$ (μmol kg^{-1})	$[CO_2]$ (μmol kg^{-1})	Ω_{Ar}	Ω_{Ca}	A_T:S
Source	Ice melt	5.9	399	399	7.926	116	385	5	9	<0.1	0.10	68
Source	UIW	31.8	2207	2132	7.954	460	2033	69	30	1.05	1.68	69
Source	UML_{20}	31.8	2257	2128	8.117	312	2008	99	20	1.51	2.42	71
Calc	UIWmix	20.3	1403	1361	8.027	267	1304	38	19	0.57	0.97	69
Calc	UML_{20}mix	29.9	2115	2000	8.114	298	1892	89	20	1.35	2.18	71

[a]The mixed result of UIW and ice melt (UIWmix) and mix of UML_{20} and ice melt (UML_{20}mix) are shown. Calculations (calc) of mixed values were performed in CO2SYS using the mean temperature of −0.5°C in end of March/April.

Table 6. Anomalously High Values of Salinity (S), Total Alkalinity (A_T) and Total Inorganic Carbon (C_T) Due to Solid $CaCO_3$ Brine Transport Were Found at Six Locations and Several Depths in the Under-Ice Water (Upper 5 m)[a]

Date (dd/mm/yyyy)	Position	Depth (m)	S	A_T (μmol kg^{-1})	C_T (μmol kg^{-1})	A_T:C_T	A_T:S
14/11/2007	70.22°N, 125.07°W	0.25	33.87	2331	2262	1.03	69
14/11/2007	70.22°N, 125.07°W	0.5	33.51	2311	2253	1.03	69
14/11/2007	70.22°N, 125.07°W	1	33.51	2307	2251	1.02	69
08/03/2008	71.10°N, 123.48°W	1	35.5	2583	2522	1.02	73
25/03/2008	71.06°N, 121.79°W	5	33.50	2384	2215	1.08	71
28/03/2008	71.06°N, 121.79°W	5	35.50	2849	2561	1.11	80

[a]These values were not included in Figure 4.

4.4. Effect of Sea-Ice Melt on the Surface Water Air-Sea CO_2 Exchange

[46] From mid-May, the ice started to melt, changing the physical and chemical properties in the sea ice, becoming more isothermal [e.g., *Geilfus et al*., 2012]. As the ice temperature increased, melt water diluted the brine and bulk-ice salinity decreased to zero in late spring. Warming of the ice resulted in larger brine volume and the CO_2 exchange changed from CO_2 outgassing in March to CO_2 uptake in May, mainly as a result of CO_2 undersaturation due to primary production (Table 4a and Figure 6b). *Geilfus et al*. [2012] estimated a net CO_2 gas flux from the atmosphere to the ice due to undersaturated fCO_2 values in brine by the end of May, which is in agreement with our results. We suggest that during melt season, solid $CaCO_3$ were released from the ice to underlying water, in accordance to the study by *Rysgaard et al*. [2013]. In our study, this is supported by the increase in [CO_3^{2-}] and the A_T:C_T ratio in the UIW in May (Figures 4f and 4i, respectively).

[47] We estimated the effect on air-sea CO_2 exchange due to addition of sea-ice melt to the surface-water carbonate system of the upper mixed layer (UML < 20 m) and the UIW, using a similar approach as *Fransson et al*. [2011]. In Table 5, we present the averages of A_T, C_T, fCO_2, and salinity in the UIW, UML, and sea ice (representing melt water) in end of March/April. We considered two scenarios in which the freshwater from the ice melt was assumed to mix down to (1) the upper 2 m (i.e., the UIW of this study) and (2) 20 m, where *Chierici et al*. [2011] observed the effect of freshwater during the same period in the same area. From the ice thickness (at the end of April) of 1.6 m, we assumed a melt-water volume of 1.6 m^3. We calculated new values of fCO_2, [CO_3^{2-}], ΩAr and ΩCa for the ice-melt-mixed surface waters (Table 5).

[48] The addition of melt water decreased both fCO_2 and Ω substantially, even when mixed down to 20 m. In the case of UIW, without the melt-water mixing, UIW would act as a CO_2 source to the atmosphere (Table 5). However, melt water mixed into the upper 2 m would result in fCO_2 undersaturation of 130 μatm and CO_2 sink, relative to atmospheric CO_2 of 395 ppm, measured in May 2008 during the same study [*Else et al*., 2012]. If the ice melt were mixed down to 20 m, compared to without ice melt, the oceanic CO_2 uptake would increase by 3 mmol m^{-2} d^{-1}, using the CO_2-flux formulation of *Wanninkhof* [1992] and an average wind speed of 6 m s^{-1} [*Spreen et al*., 2011]. Mixing the melt water into the upper 2 m, the drawdown would increase by 50 mmol m^{-2} d^{-1}.

[49] Extrapolated over much of the seasonal sea-ice zone, melt water should lead to a large infusion of C_T into the mixed layer. Due to increased sea-ice melt in summer, we estimated the hypothetic effect of melt-water carbonate system on the upper surface water and mixed layer (20 m), assuming that all sea ice will melt in one day. We estimated the changes of fCO_2 between a 20 m mixed layer with and without sea-ice melt. The rough calculation of air-sea CO_2 flux showed increased oceanic CO_2 uptake of 1.1×10^{14} gC (0.11 PgC) in one day (in theory, assuming that all summer sea ice of 3.41 million km^{-2} melted, as estimated in September 2012 by National Snow and Ice Data Centre, NSIDC). This increased CO_2 uptake would result in enhanced ocean acidification. However, this calculation neglects the capability and time for the ocean CO_2 to equilibrate with atmospheric CO_2. In this simplistic approach, we accounted only for the impact of melt water and not for biological processes, which have shown to sustain fCO_2 undersaturation throughout the winter [e.g., *Fransson et al*., 2009; *Chierici et al*., 2011; *Else et al*., 2012].

4.5. Contribution of Solid $CaCO_3$ to Underlying Water

[50] Calcium-carbonate crystals have previously been found both in Arctic and Antarctic sea ice [e.g., *Dieckmann et al*., 2008, 2010; *Rysgaard et al*., 2012, 2013; *Nomura et al*., 2013]. There is little evidence whether solid $CaCO_3$ could be directly detected in the underlying water. The density of the ikaite mineral is on average 1.8 g cm^{-3}, which is heavier than seawater (approximately 1.027 g cm^{-3}). Consequently we would assume that the crystal would sink to greater depths, if it did not dissolve. Ikaite decomposes into water and calcite above 4°C [*Assur*, 1958]. Consequently, we assume that $CaCO_3$ crystals could be transported through the water column from the ice, if the ice is porous enough [e.g., *Petrich and Eicken*, 2010] and the ikaite does not dissolve within the brines before being released to the underlying water. *Lyakhin* [1970] found circumstantial evidence that sea ice can release solid $CaCO_3$ to the underlying water and proposed that fine, colloidal carbonate salts were suspended in the Sea of Okhotsk and could remain in that state for long periods. In our study, we found anomalously high salinity, A_T, and C_T values in six UIW samples, collected on four occasions: 14 November, 8 March, 25 March, and 28 March (Table 6), which indicated brine rejection. These extreme values were not included in Figure 4 since they were regarded as anomalies. The enhanced A_T:C_T and A_T:S ratios (Table 6) in March suggest that

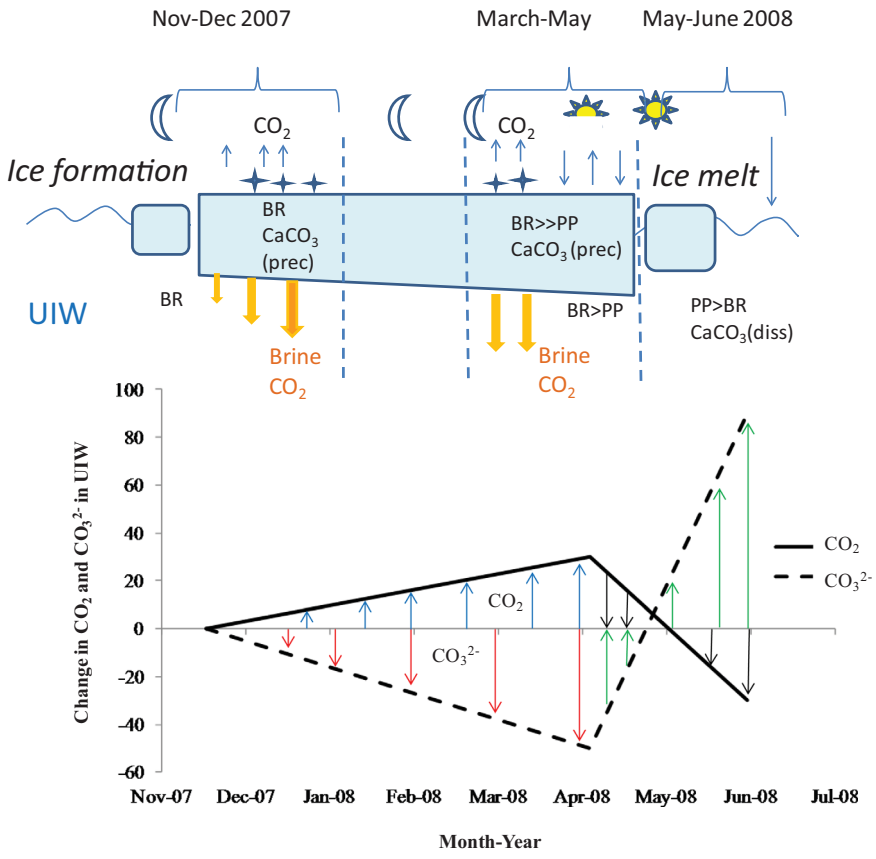

Figure 8. Conceptual model of sea-ice processes and their impacts on properties in the under-ice water (UIW). The sea-ice processes and CO_2 fluxes at the air-ice-sea interface are described for two periods: November–December 2007 (ice formation), and March–May 2008 (ice formation and onset of melt). Sea-ice processes during ice formation (the cold and dark period) are brine rejection, calcium carbonate ($CaCO_3$) precipitation (prec), bacterial respiration (BR), and primary production (PP; a minor process). Ice brines, rich in salt and inorganic carbon, move upward to form frost flowers and brine slicks on top of the ice, and downward to transport carbon from the ice to the underlying water. During ice melt, $CaCO_3$ dissolution (diss), BR, and PP occur, as the light returns. The sea-ice processes affect the under-ice water (UIW), contributing to changes in CO_2 (black solid line) and carbonate ion (CO_3^{2-}; dashed line) concentrations, and ocean acidification state.

some solid $CaCO_3$, previously precipitated within the ice, was transported with the brine (Table 3) to underlying water. Another explanation could be that $CaCO_3$ particles drained from the brine channels into the UIW during ice sampling. Certainly any suspended particulate $CaCO_3$ in our water samples would be completely dissolved prior to or during analysis, possibly contributing to the high C_T and A_T values we measured.

5. Conclusion

[51] Despite the extreme variability we observed during this study in the Amundsen Gulf, we have confirmed that sea-ice processes and brine rejection from actively freezing seawater inject carbon into underlying waters and change the chemical properties and $CaCO_3$ saturation state of Arctic Ocean ice-water interface (upper 2 m). Such sea-ice formation and brine rejection may also be a primary contributor of what we have traditionally called the global solubility pump (i.e., the ice-brine carbon pump) [*Rysgaard et al*., 2009, 2011, 2013; *Loose et al*., 2011].

[52] During ice formation from November to March in our study, CO_2-enriched brines increased [CO_2] and decreased in situ pH, [CO_3^{2-}] and ΩAr at the ice-water interface (UIW) due to brine rejection to underlying water. During the coldest period in March and April, when brine volume does not allow transport through the whole ice core, CO_2 or solid $CaCO_3$ may be trapped in the ice and dissolved during analyses. This may have caused imbalance in A_T:C_T ratio in some ice cores. During ice melt in May, [CO_3^{2-}], ΩAr and ΩCa increased due to a combination of $CaCO_3$ dissolution and primary production, as the brine volume increased with ice warming. At the same time in UIW, the $CaCO_3$ dissolved, increasing [CO_3^{2-}] and decreasing [CO_2]. The processes in sea ice and in the UIW, as well as the change in [CO_3^{2-}], [CO_2], and ΩAr in the UIW are summarized in Figure 8. The suggestions of *Nomura et al*. [2006] and *Miller et al*. [2011a] that ice-air CO_2 fluxes are directed from ice to atmosphere during ice

formation is in agreement with our results. During ice melt, CO_2 uptake is mainly explained by primary production, in agreement with the results by *Geilfus et al*. [2012], and by dissolution of solid $CaCO_3$. Bacterial respiration and $CaCO_3$ precipitation likely had an important effect on the change in sea-ice C_T in our study, and should be taken into account in future sea-ice carbon budgets. In our study, the impact of sea-ice processes was most evident in the ice-water interface. The sea-ice dynamics resulted in a five times larger seasonal amplitude of the carbonate-system parameters, in particular in [CO_3^{2-}], in the upper 2 m relative to the upper 20 m. This may have consequences for the Arctic Ocean's buffer capacity, the air-sea CO_2 flux and ocean acidification state.

[53] **Acknowledgments.** We are grateful to the captains, officers, and crew of the Canadian Coast Guard Ship (CCGS) Amundsen for their cooperation in the collection of field data, as well as to the chief scientists throughout the project. We thank Yves Gratton and his team of rosette operators for the collection and distribution of hydrographic data. Many thanks to Nes Sutherland, Debbie Armstrong, Doris Leong, Friederike Prowe, Keith Johnson, Stelly Lefort, Constance Guignard, and Kyle Simpson for their assistance with sample collection and analysis. We also thank the two anonymous referees for constructive comments improving the manuscript. This work was supported by the Swedish Research Council projects (2009–2994; 2008–6228; 2009–2994), the Royal Society of Arts and Sciences in Sweden, the Canadian Natural Science and Engineering Research Council, ArcticNet, Fisheries and Oceans Canada, and MetOcean DataSystems. This research contributes to the Canadian International Polar Year initiatives, as part of the Circumpolar Flaw Lead System study project.

References

Albert, M. R., A. M. Grannas, J. Bottenheim, P. B. Shepson, and F. E. Perron (2002), Processes and properties of snow-air transfer in the high Arctic with application to interstitial ozone at Alert, Canada, *Atmos. Environ.*, *36*(15–16), 2779–2787, doi:10.1016/S1352-2310(02)00118-8.

Alvarez-Aviles, L., W. R. Simpson, T. A. Douglas, M. Sturm, D. Perovich, and F. Domine (2008), Frost flower chemical composition during growth and its implications for aerosol production and bromine activation, *J. Geophys. Res.*, *113*, D21304, doi:10.1029/2008JD010277.

Anderson, L. G., E. Falck, E. P. Jones, S. Jutterström, and J. H. Swift (2004), Enhanced uptake of atmospheric CO_2 during freezing of seawater: A field study in Storfjorden, Svalbard, *J. Geophys. Res.*, *109*, C06004, doi:10.1029/2003JC002120.

Assur, A. (1958), Composition of sea ice and its tensile strength, in *Arctic Sea Ice, Publ. 598*, pp. 106–138, Natl. Acad. Sci. Nat. Res. Counc., Washington, D. C.

Azetsu-Scott, K., A. Clarke, K. Falkner, J. Hamilton, E. P. Jones, C. Lee, B. Petrie, S. Prinsenberg, M. Starr, and P. Yeats (2010), Calcium carbonate saturation states in the waters of the Canadian Arctic Archipelago and the Labrador Sea, *J. Geophys. Res.*, *115*, C11021, doi:10.1029/2009JC005917.

Barber, D. G., and J. M. Hanesiak, (2004), Meterological forcing of sea ice concentrations in the southern Beaufort Sea over the period 1979 to 2000, *J. Geophys. Res.*, *109*, C06014, doi:10.1029/2003JC002027.

Barber, D. G., and R. Massom (2007), The role of sea ice in Arctic and Antarctic polynyas, in *Polynyas: Windows to the World*, edited by W.O. Smith and D.G. Barber, pp. 1–54, Elsevier, Amsterdam.

Barber, D. G., M. G. Asplin, Y. Gratton, J. V. Lukovich, R. J. Galley, R. L. Raddatz, and D. Leitch (2010), The International Polar Year (IPY) Circumpolar flaw lead (CFL) system study: Overview and the physical system, *Atmos. Ocean*, *48*(4), 225–243, doi:10.3137/OC317.2010.

Carmack, E., D. Barber, J. Christensen, R. Macdonald, B. Rudels, and E. Sakshaug (2006), Climate variability and physical forcing of the food webs and the carbon budget on panarctic shelves, *Prog. Oceanogr.*, *71*, 145–181.

Chierici, M., and A. Fransson (2009), $CaCO_3$ saturation in the surface water of the Arctic Ocean: Undersaturation in freshwater influenced shelves, *Biogeosciences*, *6*, 2421–2432. [Available at www.biogeosciences. net/6/2421/2009/.]

Chierici, M., A. Fransson, B. Lansard, L. A. Miller, A. Mucci, E. Shadwick, H. Thomas, J.-E. Tremblay, and T. N. Papakyriakou (2011), The impact of biogeochemical processes and environmental factors on the calcium carbonate saturation state in the circumpolar flaw lead in the Amundsen Gulf, Arctic Ocean, *J. Geophys. Res.*, *116*, C00G09, doi:10.1029/2011JC007184.

Cox, G. F. N., and W. F. Weeks (1983), Equations for determining the gas and brine volumes in sea ice samples, *J. Glaciol.*, *29*, 306–316.

Deming, J. W. (2010), Sea ice and bacteria and viruses, in *Sea Ice*, 2nd ed., edited by D. N. Thomas and G. N. Dieckmann, chap. 7, 640 pp., Wiley-Blackwell, Oxford, U. K.

Dickson, A. G. (1990), Standard potential of the (AgCl(s) + 1/2H2 (g) = Ag(s) + HCl(aq)) cell and the dissociation constant of bisulfate ion in synthetic sea water from 273.15 to 318.15 K, *J. Chem. Thermodyn.*, *22*, 113–127.

Dickson, A. G., and F. J. Millero (1987), A comparison of the equilibrium constants for the dissociation of carbonic acid in seawater media, *Deep Sea Res., Part A*, *34*, 1733–1743, doi:10.1016/0198-0149(87)90021-5.

Dickson, A. G., C. L. Sabine, and J. R. Christian (Eds.) (2007), *Guide to Best Practices for Ocean CO_2 Measurements*, *PICES Special Publication 3*, 191 pp.

Dieckmann, G. S., G. Nehrke, S. Papadimitriou, J. Göttlicher, R. Steininger, H. Kennedy, D. Wolf-Gladrow, and D. N. Thomas (2008), Calcium carbonate as ikaite crystals in Antarctic sea ice, *Geophys. Res. Lett.*, *25*, L08501, doi:10.1029/2008GL033540.

Dieckmann, G. S., G. Nehrke, C. Uhlig, J. Göttlicher, S. Gerland, M. A. Granskog, and D. N. Thomas (2010), Brief communication: Ikaite ($CaCO_3{\cdot}6H_2O$) found in Arctic sea ice, *Cryosphere*, *4*, 227–230. [Available at: www.the-cryosphere.net/4/227/2010/doi:10.5194/tc-4-227-2010.]

Douglas, T. A., et al. (2012), Frost flowers growing in the Arctic ocean-atmosphere-sea ice-snow interface: 1. Chemical composition, *J. Geophys. Res.*, *117*, D00R09, doi:2011JD016460.

Else, B. G. T., T. N. Papakyriakou, R. J. Galley, W. M. Drennan, L. A. Miller, and H. Thomas (2011), Wintertime CO_2 fluxes in an Arctic polynya using eddy covariance: Evidence for enhanced air-sea gas transfer during ice formation, *J. Geophys. Res.*, *116*, C00G03, doi:10.1029/2010JC006760.

Else, B. G. T., T. N. Papakyriakou, R. J. Galley, A. Mucci, M. Gosselin, L. A. Miller, E. H. Shadwick, and H. Thomas (2012), Annual cycles of pCO_2sw in the southeastern Beaufort Sea: New understandings of air-sea CO_2 exchange in arctic polynya regions, *J. Geophys. Res.*, *117*, C00G13, doi:10.1029/2011JC007346.

Forest, A., et al. (2011), Biogenic carbon flows through the planktonic of the Amundsen Gulf (Arctic Ocean): A synthesis of field measurements and inverse modeling analyses, *Prog. Oceanogr.*, *91*, 410–436, doi:10.1016/j.pocean.2011.05.002.

Frankenstein, G., and R. Garner, (1967), Equations for determining the brine volume of sea ice from −0.5°C to −22.9°C, *J. Glaciol.*, *6*(48), 943–944.

Fransson, A., M. Chierici, and Y. Nojiri (2009), New insights into the spatial variability of the surface water carbon dioxide in varying sea ice conditions in the Arctic Ocean, *Cont. Shelf Res.*, *29*, 1317–1328, doi:10.1016/j.csr.2009.03.008.

Fransson, A., M. Chierici, P. L. Yager, and W. O. Smith Jr. (2011), Antarctic sea ice carbon dioxide system and controls, *J. Geophys. Res.*, *116*, C12035, doi:10.1029/2010JC006844.

Galley, R. J., E. Key, D. G. Barber, B. J. Hwang, and J. K. Ehn (2008), Spatial and temporal variability of sea ice in the southern Beaufort Sea and Amundsen Gulf: 1980–2004, *J. Geophys. Res.*, *113*, C05S95, doi:10.1029/2007JC004553.

Garrison, D. L., and K. R. Buck (1986), Organisms losses during ice melting—A serious bias in sea ice community studies, *Polar Biol.*, *6*(4), 237–239, doi:10.1007/bf00443401.

Geilfus, N.-X., G. Carnat, T. Papakyriakou, J.-L. Tison, B. Else, H. Thomas, E. Shadwick, and B. Delille (2012), Dynamics of pCO_2 and related air-ice CO_2 fluxes in the Arctic coastal zone (Amundsen Gulf, Beaufort Sea), *J. Geophys. Res.*, *117*, C00G10, doi:10.1029/2011JC007118.

Geilfus, N.-X., G. Carnat, G. S. Dieckmann, N. Halden, G. Nehrke, T. Papakyriakou, J.-L. Tison, and B. Delille (2013), First estimates of the contribution of $CaCO_3$ precipitation to the release of CO_2 to the atmosphere during young sea ice growth, *J. Geophys. Res.*, *118*, 244–255, doi:10.1029/2012JC007980.

Golden, K. M., H. Eicken, A. L. Heaton, J. Miner, D. J. Pringle, and J. Zhu (2007), Thermal evolution of permeability and microstructure in sea ice, *Geophys. Res. Lett.*, *34*, L16501, doi:10.1029/2007/GL030447.

Granfors, A., M. Andersson, M. Chierici, A. Fransson, K. Gårdfeldt, A. Torstensson, A. Wulff, and K. Abrahamsson (2013), Biogenic halocarbons in young Arctic sea ice and frost flowers, *Mar. Chem.*, *155*, 124–134.

Grasshoff, K., K. Kremling, and M. Ehrhardt (2009), *Methods of Seawater Analysis*, 3rd ed., John Wiley, New York.

Horner, R., and G. C. Schrader (1982), Relative contributions of ice algae, phytoplankton, and benthic microalgae to primary production in nearshore regions of the Beaufort Sea, *Arctic*, *35*(4), 485–503.

Hsiao, S. I. C. (1992), Dynamics of ice algae and phytoplankton in Frobisher Bay, *Polar Biol.*, *12*, 645–651.

Jones, E. P., and A. R. Coote (1981), Oceanic CO_2 produced by the precipitation of $CaCO_3$ from brines in sea ice, *J. Geophys. Res.*, *86*, 11,041–11,043.

Loose, B., W. R. McGillis, P. Schlosser, D. Perovich, and T. Takahashi (2009), Effects of freezing, growth, and ice cover on gas transport processes in laboratory seawater experiments, *Geophys. Res. Lett.*, *36*, L05603, doi:10.1029/2008GL036318.

Loose, B., P. Schlosser, D. Perovich, D. Ringelberg, D. T. Ho, T. Takahashi, J. Richter-Menge, C. M. Reynolds, W. R. McGillis, and J.-L. Tison (2010), Gas diffusion through columnar laboratory sea ice: Implications for mixed-layer ventilation of CO_2 in the seasonal ice zone, *Tellus, Ser. B*, *63*, 23–39, doi:10.1111/J.1600-0889.2010.00506.x.

Lyakhin, Y. I. (1970), Saturation of water of the Sea of Okhotsk with calcium carbonate, *Oceanology*, *10*, 789–795.

Malmgren, F. (1927), On the properties of sea ice: The Norwegian North Polar Expedition with the ''Maud'', 1918–1925, *Sci. Res.*, *1*(5), 1–67.

Massey, L. K. (2003), *Permeability Properties of Plastics and Elastomers: A Guide to Packaging and Barrier Materials*, 2nd ed., 601 pp., William Andrew, Norwich, N. Y.

Mehrbach, C., C. H. Culberson, J. H. Hawley, and R. M. Pytkowicz (1973), Measurement of the apparent dissociation constants of carbonic acid in seawater at atmospheric pressure, *Limnol. Oceanogr.*, *18*, 897–907, doi:10.4319/lo.1973.18.6.0897.

Miller, L. A., G. Carnat, B. G. T. Else, N. Sutherland, and T. N. Papakyriakou (2011a), Carbonate system evolution at the Arctic Ocean surface during autumn freeze-up, *J. Geophys. Res.*, *116*, C00G04, doi:10.1029/2011JC007143.

Miller, L. A., T. N. Papakyriakou, R. E. Collins, J. W. Deming, J. K. Ehn, R. W. Macdonald, A. Mucci, O. Owens, M. Raudsepp, and N. Sutherland (2011b), Carbon dynamics in Sea Ice: A winter flux time series, *J. Geophys. Res.*, *116*, C02028, doi:10.1029/2009JC006058.

Mucci, A. (1983), The solubility of calcite and aragonite in seawater at various salinities, temperatures and at one atmosphere pressure, *Am. J. Sci.*, *283*, 781–799.

Mucci A., B. Lansard, L. A. Miller, and T. N. Papakyriakou (2010), CO_2 fluxes across the air-sea interface in the southeastern Beaufort Sea: Ice-free period, *J. Geophys. Res.*, *115*, C04003, doi:10.1029/2009JC005330.

Ngyuen, D., and R. Maranger (2011), Respiration and bacterial carbon dynamics in Arctic sea ice, *Polar Biol.*, *34*, 1843–1855, doi:10.1007/s00300-011-1040-z.

Niemi, A., C. Michel, K. Hille, and M. Poulin (2011), Protist assemblages in winter sea ice: Setting the stage for the spring ice algal bloom, *Polar Biol.*, *34*, 1803–1817, doi:10.1007/s00300-011-1059-1.

Nomura, D., H. Yoshikawa-Inoue, and T. Toyota (2006), The effect of sea-ice growth on air-sea CO_2 flux in a tank experiment, *Tellus, Ser. B*, *58*, 418–426.

Nomura, D., P. Assmy, G. Nerhke, M. A. Granskog, M. Fischer, G. S. Dieckmann, A. Fransson, Y. Hu, and B. Schnetger (2013), Characterization of ikaite ($CaCO_3 \cdot 6H_2O$) crystals in first-year Arctic sea ice north of Svalbard, *Ann. Glaciol.*, *54*(62), 125–131, doi:10.3189/2013AoG62A034.

Orr, J. C., et al. (2005), Anthropogenic ocean acidification over the twenty-first century and its impact on calcifying organisms, *Nature*, *437*, 681–686.

Papadimitriou, S., H. Kennedy, G. Kattner, G. S. Dieckman, and D. N. Thomas (2004), Experimental evidence for carbonate precipitation and CO_2 degassing during sea ice formation, *Geochim. Cosmochim. Acta*, *68*, 1749–1761.

Perovich, D. K., and J. A. Richter-Menge (1994), Surface characteristics of lead ice, *J. Geophys. Res.*, *99*(C8), 16,341–16,350.

Petrich, C., and H. Eicken (2010), Growth, structure and properties of sea ice, in *Sea Ice*, 2nd ed., edited by D. N. Thomas and G. S. Dieckmann, pp. 23–77, Wiley-Blackwell, Oxford, U.K.

Pierrot, D., E. Lewis, and D. W. R. Wallace (2006), MS excel program developed for CO_2 system calculations, *ORNL/CDIAC-105*, Carbon Dioxide Inf. Anal. Cent., Oak Ridge Natl. Lab., U.S. Dep. of Energy, Oak Ridge, Tenn.

Pineault, S., J.-E. Tremblay, M. Gosselin, H. Thomas and E. Shadwick (2013), The isotopic signature of particulate organic C and N in bottom ice: Key influencing factors and applications for tracing the fate of ice-algae in the Arctic Ocean, *J. Geophys. Res.*, *118*, 287–300, doi:10.1029/2012JC008331.

Roy, R. N., L. N. Roy, K. M. Vogel, C. Porter-Moore, T. Pearson, C. E. Good, F. J. Millero, and D. M. Campbell (1993), The dissociation constants of carbonic acid in seawater at salinities 5–45 and temperatures 0–45°C, *Mar. Chem.*, *44*, 249–267.

Roy, R. N., L. N. Roy, K. M. Vogel, C. Porter-Moore, T. Pearson, C. E. Good, F. J. Millero, and D. M. Campbell (1994), Erratum for: The dissociation constants of carbonic acid in seawater at salinities 5–45 and temperatures 0–45°C, *Mar. Chem.*, *45*, 337.

Rudels, B., L. G. Anderson, and E. P. Jones (1996), Formation and evolution of the surface mixed layer and halocline of the Arctic Ocean, *J. Geophys. Res.*, *101*, 8807–8821.

Rysgaard, S., R. N. Glud, M. K. Sejr, J. Bendtsen, and P. B. Christensen (2007), Inorganic carbon transport during sea ice growth and decay: A carbon pump in polar seas, *J. Geophys. Res.*, *112*, C03016, doi:10.1029/2006JC003572.

Rysgaard, S., J. Bendtsen, L. T. Pedersen, H. Ramlöv, and R. N. Glud (2009), Increased CO_2 uptake due to sea ice growth and decay in Nordic Seas, *J. Geophys. Res.*, *114*, C09011, doi:10.1029/2008JC005088.

Rysgaard, S., R. N. Glud, K. Lennert, M. Cooper, N. Halden, R. J. G. Leakey, F. C. Hawthorne, and D. Barber (2012), Ikaite crystals in melting sea ice—Implications for pCO_2 and pH levels in Arctic surface waters, *Cryos. Discuss.*, *6*, 1015–1035, doi:10.5194/tdc-6-1015-2012.

Rysgaard, S., et al. (2013), Ikaite crystal distribution in winter sea ice and implications for CO_2 system dynamics. *Cryosphere*, *7*, 707–718, doi:10.5194/tc-7-707-2013.

Shadwick, E. H., et al. (2011a), Seasonal variability of the inorganic carbon system in the Amundsen Gulf region of the southeastern Beaufort Sea, *Limnol. Oceanogr.*, *56*(1), 303–322, doi:10.4319/lo.2011.56.1.0303.

Shadwick, E. H., H. Thomas, Y. Gratton, D. Leong, S. Moore, T. N. Papakyriakou, and A. E. F. Prowe (2011b), Export of Pacific carbon through the Arctic Archipelago to the North Atlantic, *Cont. Shelf Res.*, *31*, 806–816, doi:10.1016/j.csr.2011.01.014.

Song, G., H. Xie, C. Aubry, Y. Zhang, M. Gosselin, C. J. Mundy, B. Philippe, and T. N. Papakyriakou (2011), Spatiotemporal variations of dissolved organic carbon and carbon monoxide in first-year sea ice in the western Canadian Arctic, *J. Geophys. Res.*, *116*, C00G05, doi:10.1029/2010JC006867.

Spreen, G., L. Kaleschke, and G. Heygster (2008), Sea ice remote sensing using AMSR-E 89 GHz channels, *J. Geophys. Res.*, *113*, C02S03, doi:10.1029/2005JC003384.

Spreen, G., R. Kwok, and D. Menemenlis (2011), Trends in Arctic sea ice drift and role of wind forcing: 1992–2009, *Geophys. Res. Lett.*, *38*, L19501, doi:10.1029/2011GL048970.

Steinacher, M., F. Joos, T. L. Frölicher, G.-K. Plattner, and S. C. Doney (2009), Imminent ocean acidification in the Arctic projected with the NCAR global coupled carbon cycle-climate model, *Biogeosciences*, *6*, 515–533.

Thomas, D. N., and G. N. Dieckmann (2010), *Sea Ice*, 2nd ed., 640 pp., Wiley-Blackwell, Oxford, U.K.

Thomas, D. N., S. Papadimitriou, and C. Michel (2010), Biogeochemistry of sea ice, in *Sea Ice*, 2nd ed., edited by D. N. Thomas and G. S. Dieckmann, pp. 425–467, Blackwell Sci., Oxford, U.K.

Wanninkhof, R. H. (1992), The relationship between wind speed and gas exchange over the ocean, *J. Geophys. Res.*, *97*, 7373–7382.

Yamamoto-Kawai, M., F. A. McLaughlin, E. C. Carmack, S. Nishino, and K. Shimada (2009), Aragonite undersaturation in the Arctic Ocean: Effects of ocean acidification and sea ice melt, *Science*, *326*, 1098–1100, doi:10.1126/science.1174190.

Zhou, J., B. Delille, H. Eicken, M. Vancoppenolle, F. Brabant, G. Carnat, N.-X. Geilfus, T. N. Papakyriakou, B. Heinesch, J. L. Tison (2013), Physical and biogeochemical properties in landfast sea ice (Barrow, Alaska): Insights on brine and gas dynamics across seasons, *J. Geophys. Res.*, *118*(6), 3172–3189, doi:10.1002/jgrc.20232.